The Cimmerian accretionary wedge of Anarak, Central Iran

Andrea Zanchi [a,], Nadia Malaspina [a], Stefano Zanchetta [a], Fabrizio Berra [b], Luca Benciolini [c], Maria Bergomi

[a], Alessandro Cavallo [a], Hamid Reza Javadi [d], Meyssam Kouhpeyma [d]

[a] Department of Earth and Environmental Sciences, Milano-Bicocca University, Piazza della Scienza 4, 20126 Mi, Italy [b]
Dipartimento di Scienze della Terra ''A. Desio'', Università degli Studi di Milano, Mi, Italy [c] Dipartimento di Fisica, Chimica e
Ambiente, Università degli Studi di Udine, Italy [d] Geological Survey of Iran, Azadi Square, Meraj Avenue, 13185-1494 Tehran, Iran

ABSTRACT

The occurrence in Iran of several ophiolite belts dating between Late Palaeozoic to Triassic poses several questions on the possible existence of various sutures marking the closure of the Palaeotethys ocean between Eurasia and this Gondwana-derived microplate. In this scenario, the Anarak region in Central Iran still represents a conundrum. Contrasting geochronological, paleontological, paleomagnetic data and reported field evidence suggest different origins for the Anarak Metamorphic Complex (AMC). The AMC is either interpreted, as: (1) relict of an accretionary wedge developed at the Eurasia margin during the Palaeotethys subduction as part of the Cimmerian suture zone of NE Iran, displaced to Central Iran by a large counter-clockwise rotation of the central Iranian blocks; (2) autochthonous unit forming a secondary branch of the main suture zone.

Our structural, petrographic and geochemical data indicate that the AMC consists of several metamorphic units also including dismembered ''ophiolites'' which display different tectono-metamorphic evolutions. Three main ductile deformational events can be distinguished in the AMC. The Morghab and Chah Gorbeh complexes preserve a different M_1 metamorphism, characterized by blueschist relics in the S_1 foliation of the former unit, and greenschist assemblages in the latter. They share a subsequent similar D_2 deformational and M_2 metamorphic history, showing a prograde metamorphism with syn- to post-deformation growth of blueschist facies mineral assemblages on pre-existing greenschist facies associations. High pressure, low temperature (HP/LT) metamorphism responsible for the growth of sodic amphibole has been recognized also within marble lenses at the contact between the Chah Gorbeh Complex and serpentinites. Evidence of HP/LT metamorphism also occurs in glaucophane-bearing meta-pillow lavas and serpentinites, which contain antigorite and form most of the ''ophiolites'' within the AMC. Structural relationships show that the Chah Gorbeh and Morghab units and the ''ophiolites'' were tectonically coupled within an accretionary wedge before the D_2 folding stage. The other units of the AMC lack evidence of HP metamorphism in the area around Anarak, especially the Lakh Marble, a large thrust sheet that occupies the uppermost structural position in the AMC. Available radiometric ages of trondhjemite dikes and stocks that intruded the accretionary wedge, as well as our new data, constrain the subduction event at the end of the Carboniferous, before 290 Ma. These data suggest that the AMC is part of an allochthonous crustal fragment belonging to the Variscan belt developed along the southern Eurasian margin before the Cimmerian collision of Iran. Subsequent deformational events that occurred during the Mesozoic and the Cenozoic, up to the Miocene and possibly later, resulted in folding, thrusting and faulting that dismembered the original structure of the wedge accompanying its displacement to the present day position.

.

.

1. Introduction

The collisional processes taking place during the accretion of Iran to the Southern Eurasian margin have been recently described in several papers focused on the closure of the Palaeotethys suture zone (Berra et al., 2007; Horton et al., 2008; Fürsich et al., 2009; Zanchi et al., 2009a; Zanchetta et al., 2009). Evidence for the Late Triassic Cimmerian orogeny, deriving from this collision, occurs along the present-day Alborz belt and the southern portion of the Kopeh Dagh from the Mashhad region to Torbat Jam (Ruttner, 1993;Wilmsen et al., 2009, Sheikholeslami & Kouhpeyma, 2012; Zanchetta et al., 2013). According to paleogeographic reconstructions, the Iran microplate rifted off Gondwana in the Early Permian (Sengör, 1979; Berberian and King, 1981; Stampfli et al., 1991; Stampfli and Borel, 2002; Torsvik and Cocks, 2004; Angiolini et al., 2007). Iran collided with Eurasia at the beginning of the Late Triassic after the final consumption of the Palaeotethys ocean along a north-dipping subduction zone (Stöcklin, 1974; Alavi, 1991; Boulin, 1991; Ruttner, 1993; Alavi et al., 1997). The age of the collision is constrained by the deposition of the Upper Triassic to Lower Jurassic Shemshak Group in the Alborz and equivalent successions of the Kopeh Dagh (Horton et al., 2008; Fürsich et al., 2009; Wilmsen et al., 2009; Zanchi et al., 2009a), which unconformably cover the Cimmerian deformational structures. In addition, a Late Palaeozoic ''Variscan'' event occurring along the southern Eurasian margin has been documented on the northern side of the Palaeotethys suture in the Talesh Mountains, western Alborz and in the Aghdarband region of NE Iran. Carboniferous ages obtained from the Shanderman eclogites (Zanchetta et al., 2009; Omrani et al., 2013), Devonian granitoids of the Aghdarband region (Zanchetta et al., 2013) and of Darreh Anjir (Moghadam et al., 2014) in NE Iran point to geodynamic processes connected to the subduction of the Palaeotethys ocean since Early Devonian. The region east of Mashhad also records active subduction during Permian, in the arc-related units of Fariman and Darreh Anjir (Zanchetta et al., 2013) long time before the final collision of the Iran plate

This scenario, which can be followed eastward along the Paropamisus and the North Pamir ranges up to Tibet with analogous features, is complicated by the occurrence in Central Iran of similar units. These are mainly represented by the Anarak Metamorphic Complex (AMC) and reflect a Carboniferous to Triassic

accretionary history (Bagheri and Stampfli, 2008; Balini et al., 2009; Zanchi et al., 2009b). These units are exposed south of the Great Kavir Fault between Jandaq and Anarak and record the development of an active margin also testified by the Triassic arc-related sedimentary succession of Nakhlak (Balini et al., 2009) located just north of Anarak. The occurrence of these units in Central Iran has strong implications for the evolution of the Iranian plate. Davouzadeh and Weber-Diefenbach (1987) suggested that the AMC and related units are a displaced fragment of the northern branch of the Sistan suture, reaching its location after a 135 anticlockwise rotation of Central Iran (Soffel et al., 1996). Bagheri and Stampfli (2008) suggest that the AMC was part of the Palaeotethys suture originally placed east of Mashhad, reaching the present position due to the opening and successive closure of the Sabzevar ocean during the Cretaceous, accompanying the counterclockwise rotation of Central Iran. These authors proposed that the AMC resulted from a polyphase deformation and metamorphism occurred between 330 and 230 Ma, evolving from a Carboniferous ''Varsican'' event to a subsequent ''Cimmerian'' deformation during Permian and Triassic times. According to Bagheri and Stampfli (2008), the accretionary complex also includes two seamounts (Anarak and Kabudan), which were metamorphosed and accreted into the wedge during the same time interval.

On the other hand, the problem of large block rotations along vertical axes has been recently re-examined by Muttoni et al. (2009) concerning the Olenekian (Early Triassic) of Nakhlak and by Mattei et al. (2012) on the Cretaceous to Neogene units of Central Iran. Both papers show a maximum counter clockwise rotation of 45 occurring since Cretaceous, which strongly questions the previous interpretations. Nevertheless, the analysis of Jurassic rotations definitively confirmed the occurrence of large consistent counterclockwise rotations in Jurassic beds, all across Central Iran up to 70 (Mattei et al., this vol.).

The reconstruction of the Late Palaeozoic to early Mesozoic evolution of Central Iran is so complex due to the opening of Mesozoic back-arc basins, forming a continuous ophiolitic ring around the internal part of the region, and to huge displacements occurring along a complex system of intracontinental faults. Central Iran is now delimited to the north by the E–W trending left-lateral Doruneh-Great Kavir Fault interplaying with dextral N–S trending faults (Nozaem et al., 2013) delimiting different crustal blocks (Lut, Tabas, Yazd blocks), inherited by the Palaeozoic evolution of the region.

Aim of this paper is to reconstruct in detail the evolution of the Anarak region of Central Iran (Fig. 1), where the pre-Jurassic HP/LT blueschists of the AMC are better exposed. Due to the tectonic complexity of this large and still poorly known region, we have focused our work on the collection of new original data in order to improve the definition of the structural, petrologic and metamorphic history of the Anarak accretionary wedge (Sharkovski et al., 1984; Bagheri and Stampfli, 2008; Zanchi et al., 2009b). We integrated field data collected during several years of field surveys with petrological, geochemical and geochronological analyses. New radiometric ages obtained from intrusive bodies crosscutting the AMC give further constrains on the time of emplacement, metamorphism and deformation of the wedge. We have performed detailed structural observations in all the AMC units and in the overlying Cenozoic successions in order to separate the most recent deformational events.

2. Geological and structural setting of the Anarak Metamorphic Complex

The Anarak Metamorphic Complex (AMC), exposed around the town of Anarak (east of Nain), consists of an intricate polyphase thrust stack including low-grade metapelites, metabasites and marbles with a greenschist to blueschist metamorphic imprint. The AMC is associated with slivers of ultramafic rocks and metapillow lavas at HP/LT conditions (Sharkovski et al., 1984; Bagheri and Stampfli, 2008; Zanchi et al., 2009b; Buchs et al., 2013). The AMC can be followed for about 150 km forming an E–W trending belt exposed among Mesozoic and Cenozoic successions emerging from the desert between Anarak and Khur (Figs. 1 and 2). The NE– SW trending western termination of the Great Kavir Fault crosscuts the AMC to the west, juxtaposing it to the Upper Cretaceous NainBaft ophiolites (Ghasemi and Talbot, 2006), which are part of the ophiolitic ring that borders the whole Central-East Iranian Microcontinent (CEIM). The AMC is bounded to the north by the Triassic arc succession of Nakhlak (Balini et al., 2009) and to the south by the Palaeozoic to Mesozoic sequences of the Yazd block, which are very similar to the ones of the Alborz region (Wendt et al., 2005; Leven and Gorgij, 2006). The AMC is in contact to the north with the Jandaq Metamorphic Complex (JMC), containing medium to possibly high-grade Carboniferous metamorphic rocks intruded by early Mesozoic granites and pegmatites. The JMC is tectonically associated to ophiolitic slivers exposed east of Jandaq (Bagheri and Stampfli, 2008), just south of the Great Kavir Fault, and is in contact to the north with Cadomian granitoids of the Gondwanan basement of Iran. The complex also includes the Godar-e Siah Devonian to Permian succession, showing a possible Eurasian affinity (Bagheri and Stampfli, 2008), as confirmed by our new observations (Berra et al., 2014).

The AMC and JMC are completely different from the typical Palaeozoic to Triassic Gondwana-related shallow water carbonate platform successions characteristic of the Iranian plate, which extend from the Jaz Murian area to the Alborz and Kopeh Dagh regions and mark the occurrence of an active margin during the Late Palaeozoic.

Triassic deformation and metamorphism have been recently discovered also in the Posht-e Badam area, located SE of Anarak (Kargaranbafghi et al., 2012; Masoodi et al., 2013), indicating the importance of Cimmerian deformations in Central Iran.
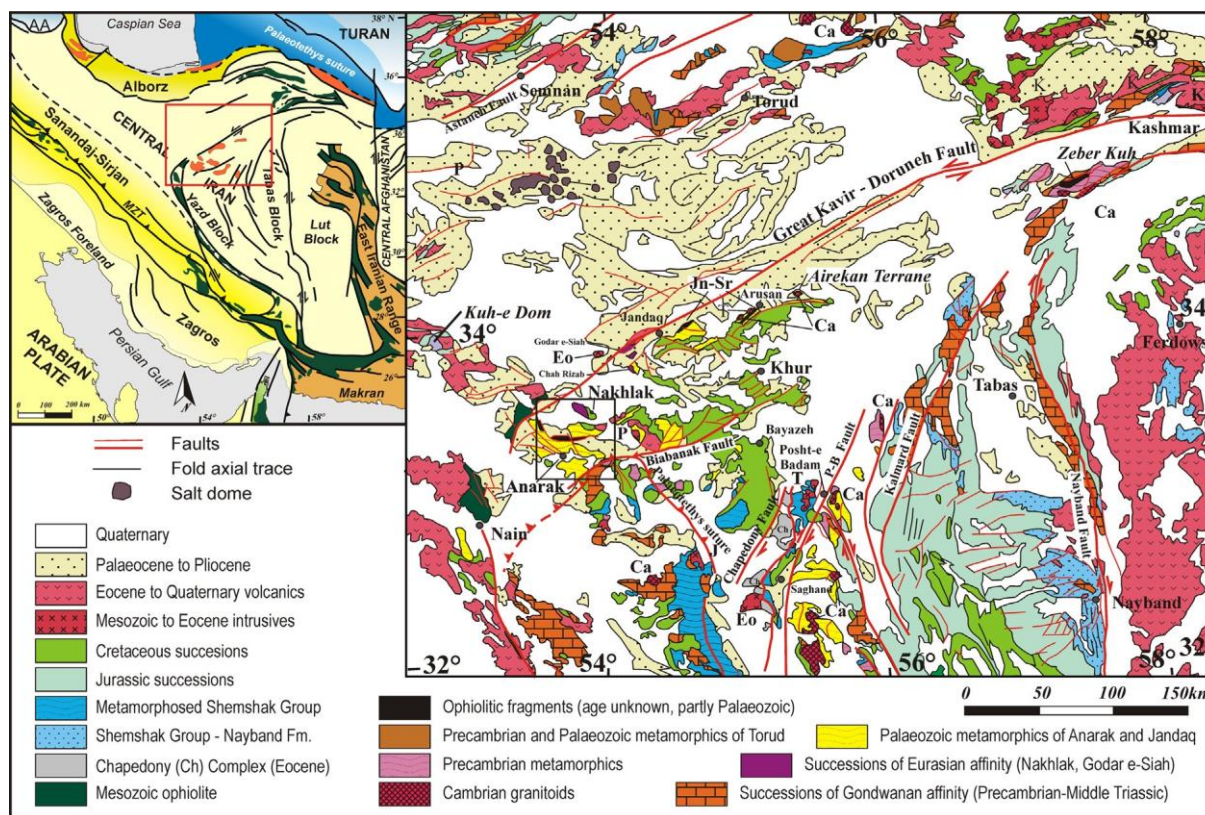
Fig. 1. Main tectonic subdivisions of Iran and general tectonic scheme of Central Iran enhancing the main tectonostratigraphic units of the area with location of the study area, modified from Zanchi et al. (2009b). Data from Torud are from Moghadam et al. (2013). Jn-Sr, ophiolitic fragments of Jandaq-Arusan; Ca, Cadomian; T, Late Triassic; J, Jurassic; K, Cretaceous; P, Palaeocene; Eo, Eocene refer to radiometric ages of granitoids.

Sharkovski et al. (1984) defined several different units within the AMC: Morghab, Chah Gorbeh, Patyar, Lakh Marble, Palhavand Gneiss, Doshak and Bayazeh (Fig. 2). They show different compositions and metamorphic evolution, and are tectonically associated to "ophiolitic" slivers of different dimensions. These units are crosscut by small mafic to felsic intrusive bodies, mainly including trondhjemite dikes and stocks, the intrusion age of which is broadly constrained to the Late Permian (Bagheri and Stampfli, 2008).

We will focus our paper on the Morghab, Chah Gorbeh, Lakh units and on the associated "ophiolites". In order to represent a synthetic structural framework of the area, we have integrated field observations in Google Earth. A general structural map of the Anarak area has been prepared showing contacts among the main structural units including trends of the metamorphic foliations (Figs. 3 and 4). Based on the results of our observations, we established some important key-points in the tectonic evolution of the area.

2.1. Morghab Complex

The Morghab Complex (MC) largely crops out through the whole area in close association with the Chah Gorbeh Complex (Figs. 2 and 3). It consists of a monotonous assemblage of lowgrade metapelites varying from phyllite to mica schist alternated with quartzite and metabasites layers, and thin marble intercalations. Garnet- biotite- mica schists locally occur close to Chah Karbouzeh (Fig. 3). Meters thick greenschist layers concordant with the main foliation occur within the unit, especially north of the Kuh-e Chah Gorbeh and in the Kuh-e Pol-e Khavand massif, south of Anarak (Fig. 2). Here they are associated with meta-rhyolite layers, which preserve original porphyritic textures given by rounded quartz phenocrysts. Amphibole-bearing gneiss also occurs in close association with the meta-rhyolite and shows a chlorite + epidote growth due to retrogression of previous associations. In the Kuhe Pol-e Khavand area, meta-rhyolites are associated with foliated fine-grained mafic layers cut by quartz veins. Also, southward with respect to these occurrences, the meta-volcanic rocks show layers characterized by cm-sized K-feldspar phenocrysts.

The unit shows a complex folding pattern due to different superposed events. Isoclinal intrafolial folds formed during a D_1 deformational event generating a S_1 axial plane schistosity. The S_1 foliation is well recognizable also in the metabasites (see Section 3.1.1). This foliation was refolded by a second D_2 pervasive event forming tight to isoclinal folds (Fig. 5a and b). A marked greenschist facies metamorphic imprint accompanies the development of the S_2 foliation associated with this second superposed fold system. Quartz aggregates often define a mineral lineation both parallel and orthogonal to the D_2 fold axes. Variable trend and plunge of the D_2 folds suggest the occurrence of a third important D_3 large scale folding event superposed on previous structures (Fig. 4) and forming open to closed folds.

In spite of the strong transposition of the primary foliation S_0, abrupt transitions from metapelitic to metapsammitic layers may reflect some original lithostratigraphic features of this dominantly meta-sedimentary unit.

The Morghab Complex also outcrops west of Anarak, at Kuh Darreh Anjir where it shows similar structural characters (AJ12, Fig. 2).

The boundary between the Morghab Complex and the Chah Gorbeh Complex is generally concordant (Fig. 4), as well as the main regional foliations of the two units, due to the D_2 folding stage. In addition, both units were refolded by an important D3 deformational event.
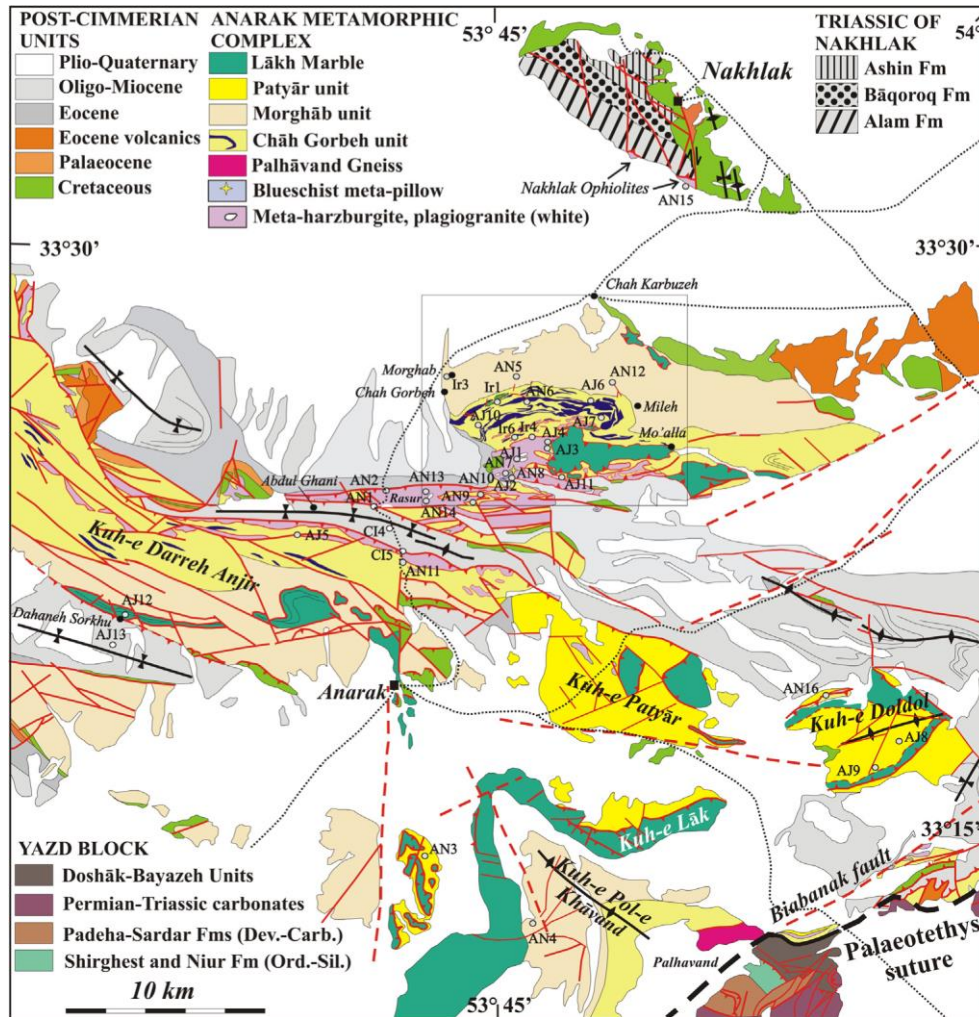
Fig. 2. Schematic geological map of the Anarak region based on the 100,000 geological map of Anarak. Modified from Zanchi et al. (2009b), according to our original data with location of mesoscopic structural observations.

Bagheri and Stampfli (2008) interpreted the Morghab Complex as a ''Variscan accretionary unit'' based on $^{40}Ar–^{39}Ar$ muscovite ages ranging between 320 and 335 Ma.

2.2. Chah Gorbeh Complex

The Chah Gorbeh Complex (CGC) consists of quartzite-rich phyllite, micaschist, and metabasites interlayered with thick marble layers (Figs. 2 and 3) and calc-schists. This unit is very similar in composition to the MC with the main exception given by the occurrence of large dolomite and calcite marble layers forming a scenic landscape with carbonate peaks and sharp ridges showing high rock walls. Meta-cherts occur within marble layers and along their contacts. Some meters thick greenschist facies metabasite intercalations are present in the unit. They show coarse albite porphyroblasts often replaced by pseudomorphs of epidote aggregates, along a foliation given by quartz ribbons, chlorite and blue amphibole needles. NE of Anarak, from Chah Gorbeh to the Mileh mine, the CGC occurs in an upper structural position resting with complex and folded contacts on the ''ophiolites''. N and NW of Anarak the CGC forms tectonic slices interleaved to the main serpentinite bodies. The CGC also outcrops south of Anarak along the boundary with the Yazd block marking the Palaeotethys suture zone.

The CGC is generally concordant with the MC, at least in the area around Chah Gorbeh (Fig. 3), where no important fault zones are evident between the two units. We have observed a tectonic contact with the Lakh Marble in most of the studied sites, especially in the external part of the Kuh-e Doldol area south of Anarak where the Lakh Marble overthrusts both the CGC and Patyar units as well as around the Kuh-e Chah Gorbeh (Fig. 2).

The Chah Gorbeh Complex also shows two main foliations related to two superposed folding events with mineral associations partially different from the ones recognized in the MC. A S_1 greenschist facies foliation is often evident at the mesoscale and is well recognizable at the microscale, where it is preserved in the cores of albite and epidote porphyroclasts (see Sections 3.2.1 and 3.2.2). This is related to F_1 intrafolial mesocopic folds developed at lowgrade metamorphic conditions. D_1 folds were followed by a second folding stage (Fig. 5c and d), related to the D_2 deformation, associated to a S_2 foliation, formed by chlorite, white mica, albite and blue amphibole, which records a prograde transition from greenschist to blueschist facies conditions. The D_2 deformation seems to be common to both the CGC

and MC units. A marked mineral lineation given by quartz aggregates with trends similar to the ones displayed by the MC is also evident in the unit and refers to the D2 folding stage.
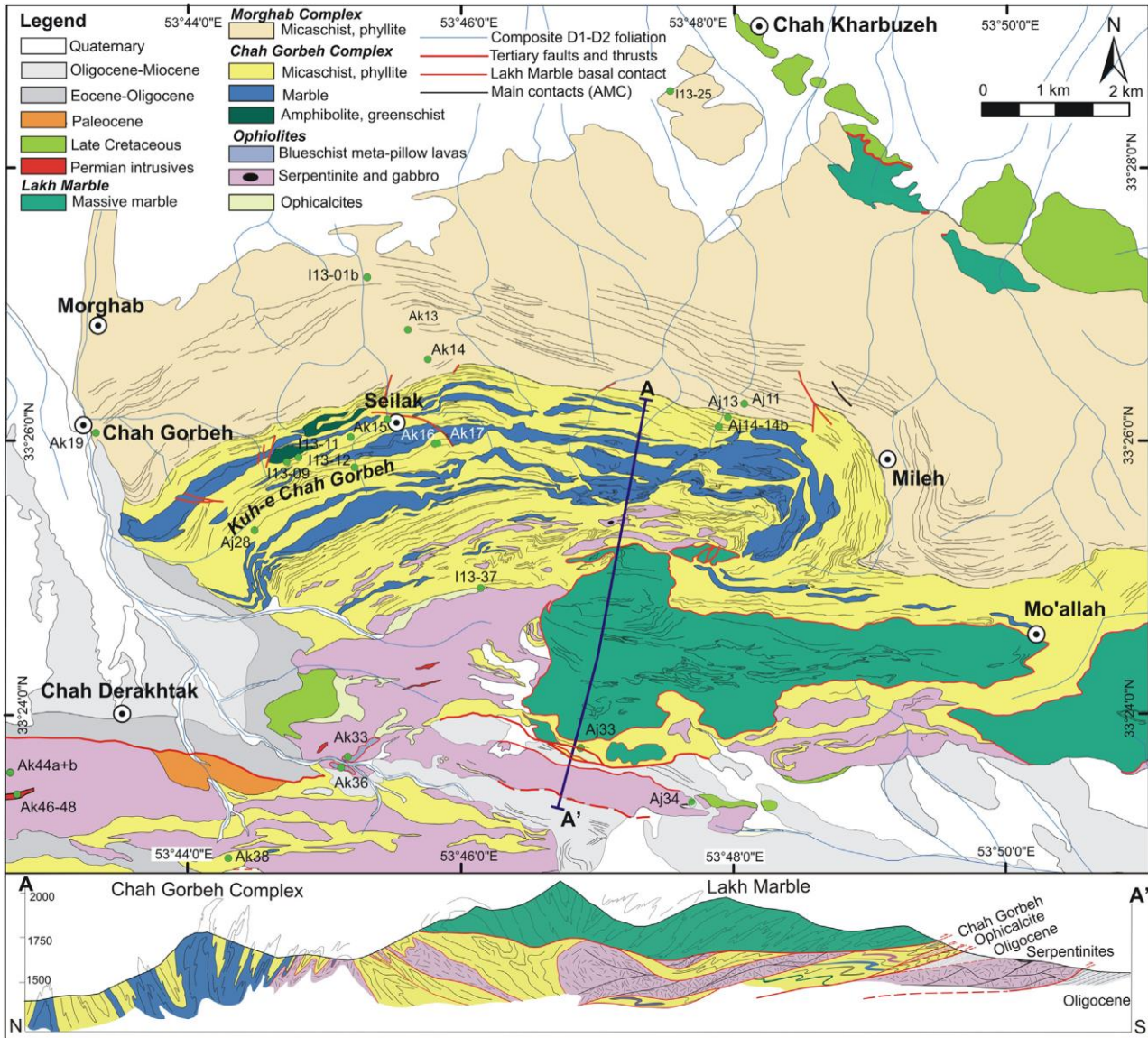

Fig. 3. Geological map of the northern part of the Anarak Metamorphic Complex (AMC) with location of the analyzed samples. The map is based on fieldwork and photointerpretation with Google Earth. The map also shows an interpretative N–S trending cross-section summarizing the main structural features of the area.

Isoclinal folds with axes varying from sub-horizontal to vertical, superposed on a previous foliation, occur in this unit also around Seilak (Fig. 4), where D2 folds are well exposed and more visible by differences in lithological composition. Large E–W trending isoclinal vertical folds affecting the marble layers are also evident in the Chah Gorbeh unit close to the Mileh abandoned mine. D2 isoclinal folds also affect the contacts between serpentinites of the ophiolitic units, which coupled before this major deformational event (Site Ir7, Fig. 6).

A syn- to post-kinematic blueschist facies metamorphic imprint is associated to the D2 deformation phase. HP mineral assemblages also occur in textural equilibrium within shear zones formed along the contacts between the CGC and deformed serpentinite slivers (see Section 3). This suggests that the two units paired at relatively HP/LT conditions during subduction.

The D3 folding event is also evident in this unit as in the MC especially in the area east of the Mileh mine (Fig. 7). Reorientation and growth of fine-grained white micas may occur along the axial planes of D3 folds.

Bagheri and Stampfli (2008) proposed an Early Permian age (285 Ma) for the blueschist facies metamorphism in the CGC, based on a poorly constrained $^{40}Ar/^{39}Ar$ radiometric dating of Na-amphibole, separated from a blueschist sample around Seilak (Fig. 3). Based on this radiometric age, the same authors interpreted the CGC as unit independent from the MC, recording a Late Permian to Triassic history of accretion post-dating the Variscan deformation of the MC.

2.3. Lakh Marble

The Lakh Marble (LM) widely extends around Anarak (Figs. 2 and 3) from Kuh-e Chah Gorbeh to the Doldol Mountains (Sharkovski et al., 1984). It consists of massive to bedded strongly recrystallized marble, locally deformed by polyphase isoclinal folds. In several sectors, especially around the Lakh ridges, the unit shows a weak

deformation, still preserving sedimentary structures as bedding, intraformational paracongolomerates and fossils. The carbonates here include fine-grained deposits with dispersed bioclasts as crinoids, large gastropods, brachiopods and possibly corals remains.

The base of the unit is a thrust fault, juxtaposing the LM to the Patyar Complex and to the MC south of Anarak (Fig. 8a), whereas to the north it is stacked upon the CGC and the MC with complex tectonic contacts (Fig. 8b and c). South of Kuh-e Chah Gorbeh the main thrust flooring the LM shows duplex structures with small imbricates consisting of the underlying rocks of the CGC and of cataclastic serpentinite, which override the Oligocene succession. The western portion of the LM floor thrust forms a left-lateral ramp showing an intensive brittle deformation affecting the serpentinites and superposed to the isoclinal folds of the CGC (Site AJ4, Figs. 4 and 8c).
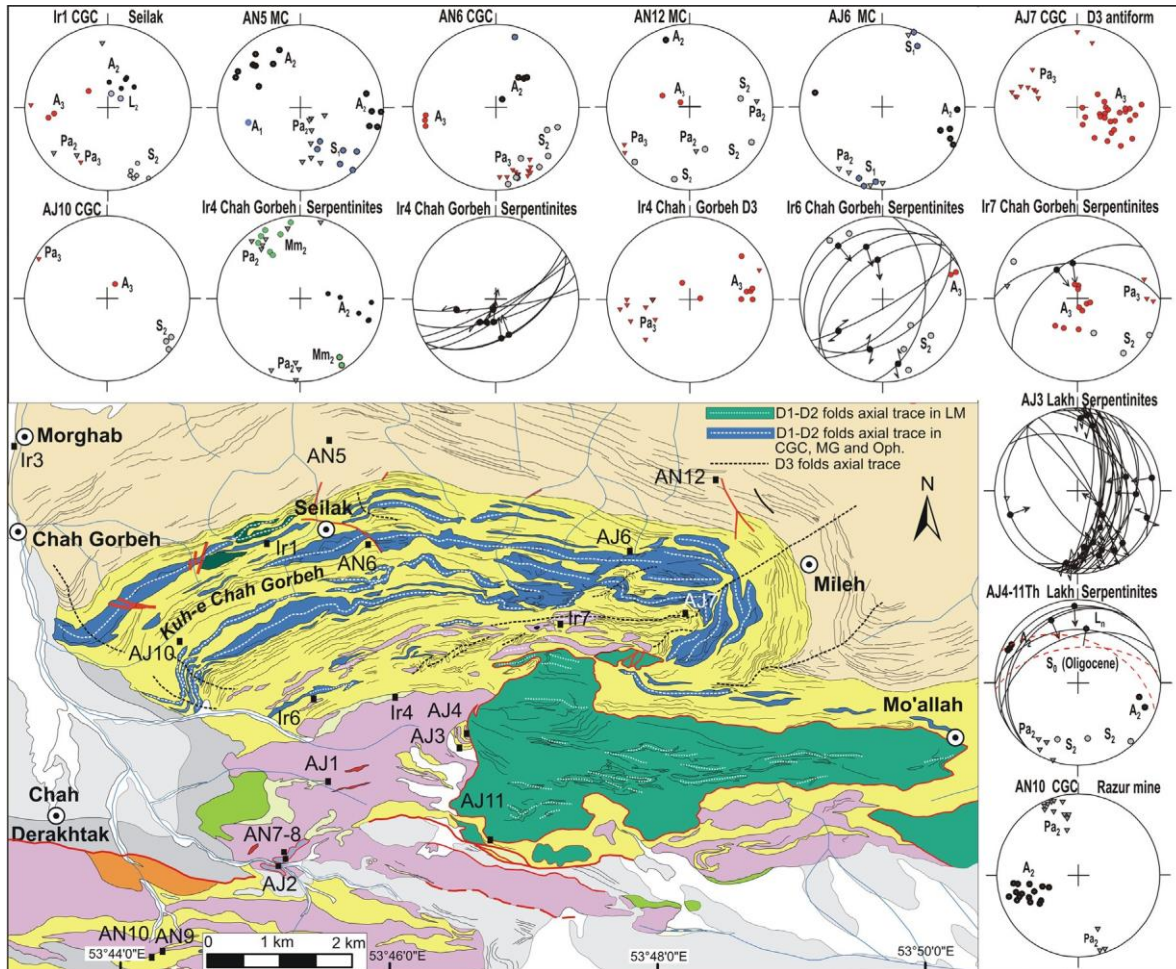

Fig. 4. Structural map of the same area of previous Fig. 3, with location of the studied sites and stereoplot representations of classified tectonic structures. Letters indicate the type of structure followed by a subscript related to the established relative chronology (A: fold axis; Pa: pole to fold axial plane; L: mineral lineation; S: foliation; Mm: mylonitic foliation). Different symbols relate to the three main ductile deformational events (D_1, D_2 and D_3) and to following brittle deformations.

In the Kuh-e Chah Gorbeh area, the floor thrust of this unit, as well as the serpentinites and the CGC, are deformed by the D_3 folding stage.

Thick calc-mylonitic layers often occur in the basal part of the unit close to the floor thrust. A brittle imprint is generally superposed on the ductile structures due to N-S compression (Site AJ11, Fig. 4). A well-defined mineral lineation, given by a preferred orientation of calcite, often occurs, especially in the southern part of the area around the Doldol Mountains, where the Lakh Marble forms faulted klippen resting on the Pathyar Complex. Subsequent recrystallization anneals mylonite fabrics along other segments of the contacts.

The age of the Lakh Marble is poorly constrained; it represents one of the major unsolved problems of the geology of the area. Sharkovski et al. (1984) report the occurrence of archeocyathids in the eastern Kuh-e-Lakh massif and in the Khur area, suggesting an Early Cambrian age for this part of the unit. Nevertheless, the finding of large crinoids in different parts of the unit and large gastropods, brachiopods and possibly corals suggests a younger age. In addition, facies association and carbonate volume suggest an age younger than Early Cambrian for the unit, as carbonate production during that period was limited to carbonate mounds or thick microbial successions. We thus propose a possible Late Palaeozoic age, in agreement with Bagheri and Stampfli (2008). We were unable to find archeocyathids in the described localities in the Lakh Mountains and at Khur (Sharkovski et al., 1984), where isoclinal folding accompanied by strong recrystallization of the marble layers makes difficult their preservation.

The basal tectonic contact and the occurrence of different units in the footwall of the main thrust surface support the interpretation of the Lakh Marble as a huge thrust nappe. The present-day distribution of the unit suggests that the thrust moved over a distance of tens of kilometers (Figs. 2 and 8). The allochthonous position of the LM is especially evident around the Doldol Mountains, where marble klippen show a very steep to vertical foliation. They overthrust the Patyar Complex, which shows polyphase folding and metamorphism.

2.4. Ultramafic rocks

Several tectonic slices and patches of ultramafic rocks outcrop in the area around Anarak. They occur in two structural settings: (1) they form relatively small tectonic slices intimately associated with the CGC along isoclinal folds and shear zones; (2) they occur in a lower structural position, forming large and continuous imbricated thrust slices underlying the CGC (Fig. 3). Important thrust stacking and brittle overprinting of the main tectonic contacts occurred at the end of the Mesozoic and during the Cenozoic, hampering the original geometrical and structural relationships between these units.
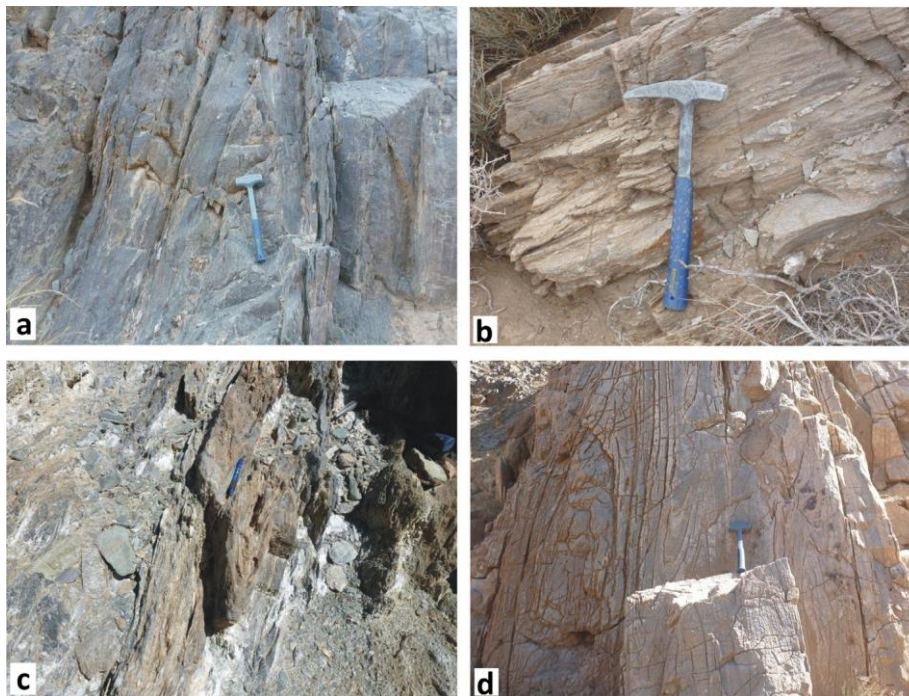

Fig. 5. Isoclinal folds in the Morghab and Chah Gorbeh complexes. D_2 isoclinal folds within the Chah Gorbeh Complex show the same style of the D_2 folds in the Morghab Complex. (a) Upright tight fold in greenschist metabasites (MC) close to the contact between the Morghab and the Chah Gorbeh units, SE of Mileh, site AJ6. (b) Sub-isoclinal folds in a paragneiss at site An5 (MC). (c) Vertical isoclinal folds at site AN6 (CGC), 1 km east of Seilak south of Chah Karbuzeh, top view of the outcrop. (d) Sub-horizontal isoclinal folds in marble layers (CGC) NE of the Mileh mine close to site AJ6. Attitude variations of the fold axial planes is due to the D_3 event. Sites location in Figs. 3 and 4.

Fig. 6. D_2 isoclinal folds between Marble layer of the CGC and the serpentinites, at site Ir7 (Fig. 4).

In the area around Kuh-e Chah Gorbeh, north of Anarak, ultramafic rocks chiefly consist of serpentinites, with minor orthopyroxene relics of spinel peridotites. Serpentinites display a schistose texture with isolated massive domains, where the primary phase assemblage consists of olivine, minor clinopyroxene relics and mm-sized orthopyroxene. This suggests that the original peridotite was harzburgitic in composition. Near the Chah Derakhtak quarry (Fig. 3), serpentinites show a massive texture, cut by brittle shear zones with large chrysotile fibers grown along fractures. Here the ultramafic rocks preserve relics of coarse ortho and clinopyroxene. In the easternmost side of the ultramafic lens, serpentinites preserve relics of harzburgite peridotite with mylonitic texture, characterized by coarse-grained orthopyoxene, typical of high temperature equilibration. In this outcrop, serpentinites host slices of carbonate rocks, which do not record any chemical interaction with the serpentinites. On the other hand, some serpentinite lenses occurring in carbonate rocks show white clinopyroxene grains indicating either a possible enrichment in Ca provided by the associated carbonates during fluid-mediated chemical exchange, or later weathering processes.

Small E–W trending elongated lenses of serpentinites exposed south of Kuh-e Chah Gorbeh are closely associated with the marble layers of the CGC, forming tight to isoclinal folds related to the D_2 deformation stage. Ultramafic bodies are here highly sheared, showing a pervasive serpentinization where no relics can be recognized.

They have been uplifted within the core of one of the main D_3 antiform deforming previous ductile structures (Fig. 7). Larger serpentinite bodies cropping out in the upper part of the Chah Gorbeh catchment show thick shear zones with boudinaged serpentinites in a carbonate matrix overprinted by cataclasites.

In the Patyar Mountains, small slices of cataclastic serpentinitic bodies occur along the new road from Anarak to Tabas. Talc-rich shear zones indicating high temperature conditions separate sediments and serpentinites. In the Doldol area, isolated outcrops are exposed along the footwall of the Lakh Marble nappe. In these occurrences ultramafic rocks are completely serpentinized and do not preserve any peridotite relic.

2.5. Blueschist pillow meta-basalts

Blueschist meta-basalts with well-preserved pillow structures occur north of Anarak (Zanchi et al., 2009b; Torabi, 2011; Buchs et al., 2013). They form isolated tectonic slices within an intricate S-verging imbricate thrust stack including catacalastic foliated serpentinites with ophicalcite-rich fault zones at the base, and pillow lavas at the top. Thick mylonitic layers developed under

blueschist conditions separate pillow meta-basalts (Figs. 9 and 10). They are in turn tectonically juxtaposed to undeformed trondhjemites (Torabi, 2012), thus postdating deformation and HP/LT metamorphism, as they show perfectly preserved magmatic textures.
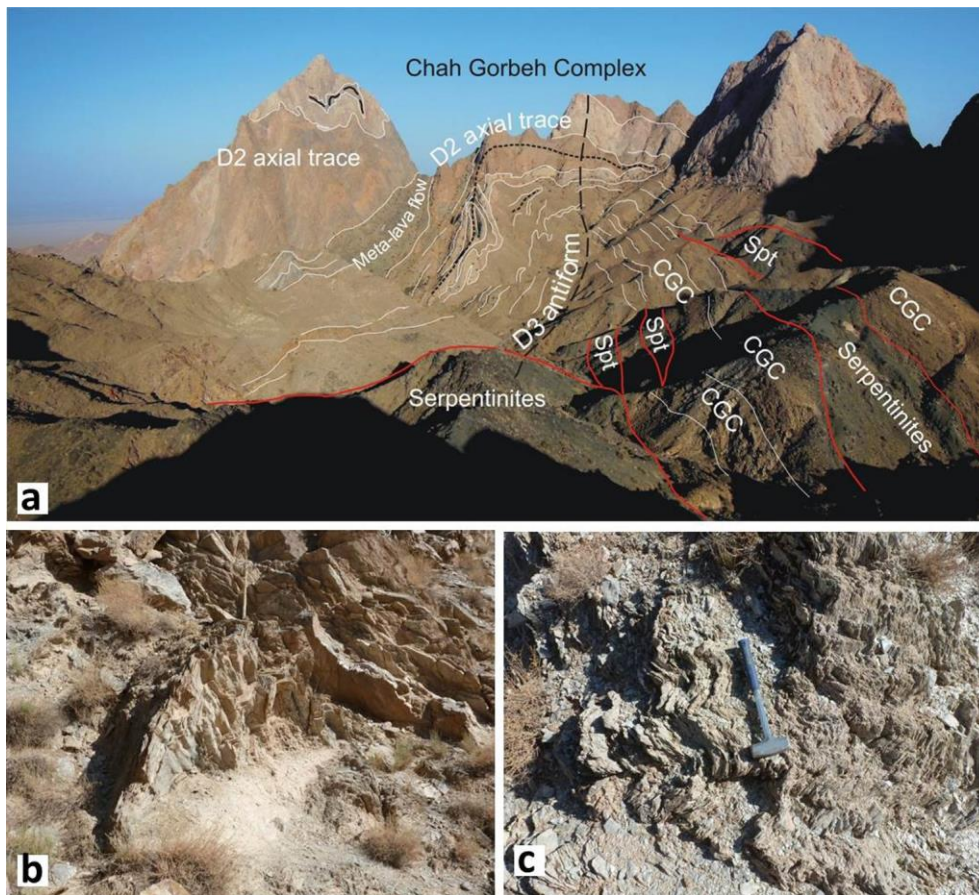
Fig. 7. (a) D_2–D_3 interference pattern within the nose of the Mileh antiform. Note the occurrence of serpentinites within the core of the fold. Compare with the structural map of Fig. 4. The photo points to the east from site I37. (b and c) Parasitic folds belonging to the D_3 antifom at site AJ7 within the core of the Mileh plunging fold.
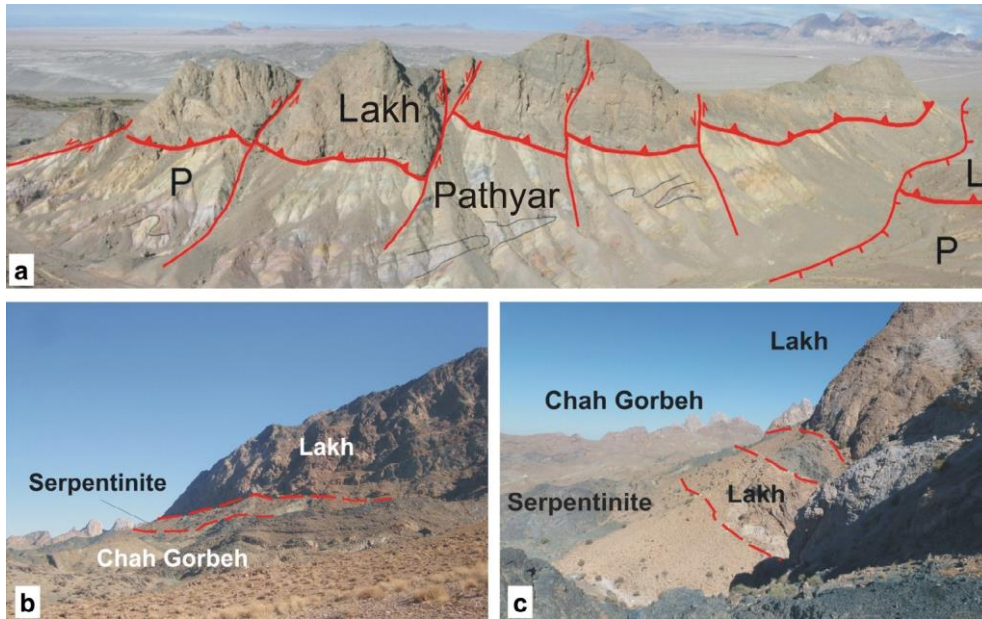
Fig. 8. Panoramic view of different outcrops of the Lakh Marble (L) overthrusting different units. (a) A faulted klippe of the Lakh Marble overthrusts the Patyar Complex (P) showing isoclinal folds south of Anarak. (b and c) The western part of the contact between the Lakh Marble and the serpentinites south of Kuh-e Chah Gorbeh. (b) Duplex structures with serpentinite slivers resting on top of the Chah Gorbeh metapelites below the floor thrust of the LM. (c) Complex tectonic repetitions along the main thrust surface, moving to the N of site AJ4 (Fig. 4).
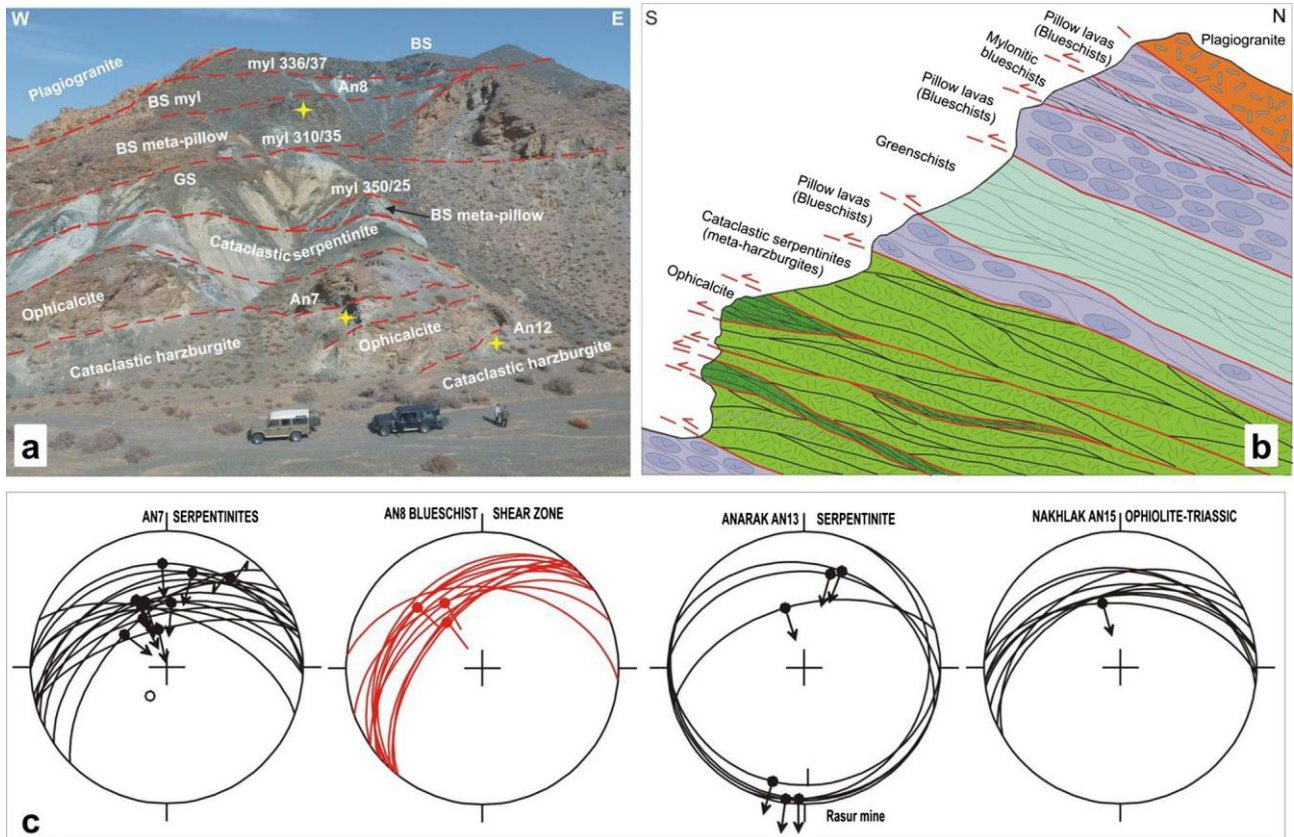
Fig. 9. (a) Blueschists exposures at site AN7, AN8, AJ2, N of Anarak on top of cataclastic serpentinites. (b) Cross section of the outcrop shown in (a), possibly representing the remnant of an accretionary wedge. (c) Mesoscopic data on the S-verging thrust planes and ductile shear zones (red) deforming the blueschist succession and comparison with S-verging thrust planes at the Razur mine (An13) and Nakhlak (An15). (For interpretation of the references to colour in this figure legend, the reader is referred to the web version of this article.)
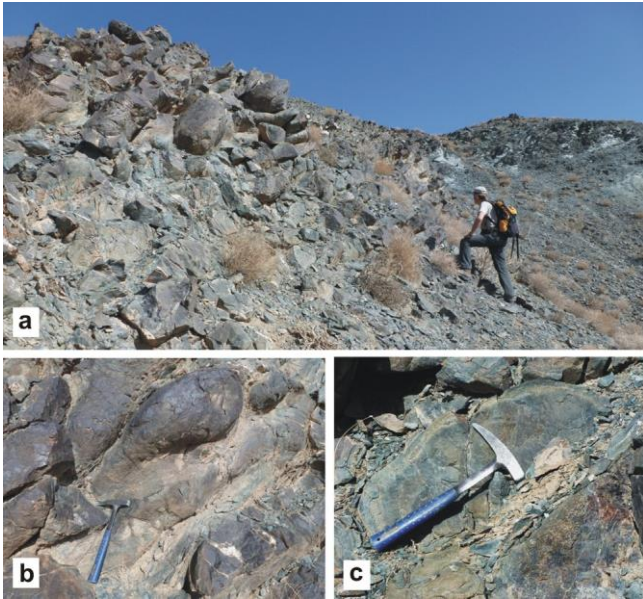
Fig. 10. Close view of blueschist pillow basalts of Fig. 9. (a) Preserved pillow lavas are well recognizable in the outcrop. (b) Elongated pillows at the base of the outcrop. (c) Preserved internal texture of a pillow.

Fig. 11. Trondhjemite dike intruding the serpentinites exposed south of the Rasur mine (Fig. 2).

Pillow basalts are often preserved as rounded lenses, but some bodies are strongly deformed. They display a marked foliation given by chlorite and superposed Na-amphibole (see Section 3.3), or alternatively preserve a prograde HP/LT mineral assemblage, that statically grew on previous greenschist facies parageneses (see Section 3.3). Small veins filled by white mica and epidote crosscut these rocks. Although previous authors considered these rocks as part of the Chah Gorbeh Complex, we propose that the pillow-lavas form an independent unit, which may eventually belong to the ''ophiolite'' rather than to the CGC, as they totally lack its complex polyphase tectono-metamorphic evolution.

Table 1
Sample description and location.

Sample	Tectonic unit	Rock type	Mineralogy																					Coordinates	
			Qtz	Pl	Wm	Bt	Grt	Ep	Cc	Chl	Stp	Rt	Ttn	Amp	Serp	Ol	Cpx	Tc	Mt	ox	Ap	Zr	Pyr	Latitude (N)	Longitude (E)
AK31	Ultramafic rocks	Serpentinite							x						x	x	x		x					$3323^{0}42^{00}$	$5345^{0}03^{00}$
AK44	Ultramafic rocks	Serpentinite													x				x					$3323^{0}40^{00}$	$5342^{0}40^{00}$
I13-38	Ultramafic rocks	Serpentinite													x	x			x					$3323^{0}29^{00}$	$5341^{0}35^{00}$
I13-52	Ultramafic rocks	Serpentinite							x	x					x		x	x	x					$3324^{0}52^{00}$	$5345^{0}26^{00}$
I13-55	Ultramafic rocks	Serpentinite								x					x				x					$3324^{0}56^{00}$	$5345^{0}27^{00}$
I13-56	Ultramafic rocks	Serpentinite							x	x					x				x					$3324^{0}56^{00}$	$5345^{0}27^{00}$
I13-63	Ultramafic rocks	Serpentinite													x	x			x					$3325^{0}25^{00}$	$5347^{0}07^{00}$
AK33A	Pillow meta-basalts	Blueschist		x	x			x		x			x	x					x		x			$3323^{0}41^{00}$	$5345^{0}10^{00}$
AK33B	Pillow meta-basalts	Blueschist		x	x			x		x			x	x										$3323^{0}41^{00}$	$5345^{0}10^{00}$
AK36	Pillow meta-basalts	Blueschist		x	x			x		x			x	x					x		x			$3323^{0}36^{00}$	$5345^{0}07^{00}$
I13-06	Chah Gorbeh	Amphibolite		x	x			x	x	x			x	x					x			x		$3326^{0}02^{00}$	$5345^{0}11^{00}$
I13-09	Chah Gorbeh	Blueschist	x	x	x			x	x	x			x	x					x		x			$3325^{0}53^{00}$	$5344^{0}48^{00}$
I13-11	Chah Gorbeh	Blueschist	x	x	x			x		x			x	x					x		x			$3325^{0}51^{00}$	$5344^{0}43^{00}$
AJ13	Chah Gorbeh	Epidote–chlorite schist	x	x	x			x		x	x								x				x	$3326^{0}10^{00}$	$5347^{0}57^{00}$

Table 2

Sample	Locality	Rock type	1	2	3	4	5	6	7	8	9	10	11	12	13	14	15	Latitude	Longitude
AJ14	Chah Gorbeh	Two mica paragneiss	x	x	x	x		x		x	x		x		x			$3326^{\circ}06^{00}$	$5347^{\circ}53^{00}$
AJ28b	Chah Gorbeh	Quartzschist	x	x	x	x		x				x			x		x	$3325^{\circ}21^{00}$	$5344^{\circ}29^{00}$
AJ33	Chah Gorbeh	Micaschist	x	x	x		x	x		x					x			$3323^{\circ}49^{00}$	$5346^{\circ}38^{00}$
AK15	Chah Gorbeh	Micaschist	x	x	x		x			x			x		x	x		$3326^{\circ}09^{00}$	$5345^{\circ}28^{00}$
AK16	Chah Gorbeh	Micaschist	x	x	x	x		x		x					x	x		$3325^{\circ}59^{00}$	$5345^{\circ}48^{00}$
AK17	Chah Gorbeh	Epidote–chlorite schist	x	x	x	x		x		x					x	x	x	$3325^{\circ}29^{00}$	$5345^{\circ}48^{00}$
AK38	Chah Gorbeh	Carbonate-bearing micaschist	x	x	x	x			x						x			$3322^{\circ}57^{00}$	$5344^{\circ}18^{00}$
I13-12	Chah Gorbeh	Micaschist	x	x	x			x		x	x				x	x		$3325^{\circ}48^{00}$	$5345^{\circ}13^{00}$
I13-37	Chah Gorbeh	Marble	x		x				x	x				x	x			$3324^{\circ}55^{00}$	$5346^{\circ}09^{00}$
AK14A	Morghab	Greenschist (Blueschist relicts)		x	x			x		x		x	x		x	x		$3326^{\circ}36^{00}$	$5345^{\circ}45^{00}$
AK19B	Morghab	Greenschist (Blueschist relicts)		x	x			x		x		x	x		x			$3326^{\circ}03^{00}$	$5343^{\circ}19^{00}$
AJ11	Morghab	Quartzschist	x	x	x	x				x					x			$3326^{\circ}16^{00}$	$5348^{\circ}04^{00}$
AK13	Morghab	Epidote–chlorite schist	x	x	x			x		x			x		x	x		$3326^{\circ}49^{00}$	$5345^{\circ}37^{00}$
I13-01b	Morghab	Epidote–chlorite schist	x	x	x			x		x					x	x		$3327^{\circ}12^{00}$	$5345^{\circ}19^{00}$
I13-25	Morghab	Garnet micaschist	x	x	x	x	x			x					x	x	x	$3328^{\circ}34^{00}$	$5347^{\circ}32^{00}$

Notes: Mineral abbreviations. Amp: amphibole; Ap: apatite; Bt: biotite; Cc: calcite; Chl: chlorite; Cpx: clinopyroxene; Ep: epidote; Grt: garnet; Mt: magnetite; Ol: olivine; ox: Fe–Ti oxides; Pl: plagioclase; Pyr: pyrite; Qtz: quartz; Rt: rutile; Serp: serpentine; Stp: stilpnomelane; Tc: talc; Ttn: titanite; Wm: white mica; Zr: zircon.

Amphibole mineral chemistry. Representative major element compositions (wt.% oxide) and recalculated structural formulae of amphiboles of metabasites from MC, CGC and Ophiolite unit (metapillow).

Unit	Morghab								Chah Gorbeh					Ophiolite unit					
Sample	AK19B				AK14A				I1309		I1311			AK36A		AK33A		AK33B	
	Amp_1 (inc in Ep_2)	Amp_1 (inc in Ep_2)	Amp_2 (core)	Amp_2 (rim)	Amp_1 (inc in Ab)	Amp_1 (inc in Ep_2)	Amp_2 (core)	Amp_2 (rim)	Amp_2 (core)	Amp_2 (rim)	Amp_1	Amp_2 (core)	Amp_2 (rim)	Amp_2 (core)	Amp_2 (rim)	Amp_1 (fine)	Amp_2 (coarse)	Amp_2 (core)	Amp_2 (rim)
SiO_2	56.30	56.31	52.99	49.39	52.40	56.87	53.45	50.97	56.12	55.61	50.12	54.22	55.66	56.10	55.63	55.17	55.59	55.71	55.89
TiO_2	0.02	0.04	0.05	0.16	0.02	0.04	0.02	0.06	0.11	0.08	0.04	0.20	0.17	0.05	0.10	0.08	0.05	0.03	0.06
Al_2O_3	7.77	7.64	2.43	6.22	3.20	8.26	2.37	4.63	8.60	7.66	4.71	8.20	8.56	2.43	1.67	1.61	2.10	2.13	1.99
Cr_2O_3	0.00	0.00	0.03	0.02	0.00	0.02	0.05	0.02	0.04	0.06	0.01	0.00	0.03	0.06	0.08	0.10	0.07	0.08	0.07
FeO^*	17.12	16.90	15.13	17.90	17.35	17.92	15.96	19.52	19.63	19.59	19.71	19.64	18.90	19.97	19.32	18.78	21.03	19.11	19.70
MgO	7.75	8.15	13.72	10.90	11.38	6.61	12.99	10.19	6.21	7.00	10.77	7.01	6.71	10.03	10.63	11.45	9.75	10.66	10.42
MnO	0.20	0.14	0.35	0.38	0.28	0.25	0.25	0.36	0.11	0.08	0.23	0.18	0.10	0.12	0.18	0.15	0.12	0.11	0.13
CaO	0.71	0.93	11.06	9.06	9.96	0.44	10.64	8.96	0.54	0.78	9.47	0.76	0.65	1.08	2.95	4.92	1.51	2.03	1.57
Na_2O	6.91	6.90	1.01	2.54	1.75	7.07	1.21	2.48	7.35	7.23	2.24	7.00	7.13	6.71	5.85	4.64	6.40	6.19	6.39
K_2O	0.01	0.01	0.09	0.27	0.09	0.02	0.13	0.25	0.01	0.02	0.36	0.01	0.03	0.01	0.03	0.10	0.05	0.04	0.04
Total	96.79	97.01	96.85	96.84	96.43	97.50	97.07	97.44	98.72	98.11	97.66	97.23	97.94	96.56	96.45	97.00	96.66	96.10	96.27
Si	8.03	8.01	7.72	7.31	7.72	8.06	7.78	7.52	7.93	7.93	7.41	7.82	7.91	8.18	8.14	8.04	8.15	8.16	8.18
Ti	0.00	0.00	0.01	0.02	0.00	0.00	0.00	0.01	0.01	0.01	0.00	0.02	0.02	0.01	0.01	0.01	0.01	0.00	0.01
Al	1.31	1.28	0.42	1.08	0.56	1.38	0.41	0.81	1.43	1.29	0.82	1.39	1.43	0.42	0.29	0.28	0.36	0.37	0.34
Cr	0.00	0.00	0.00	0.00	0.00	0.00	0.01	0.00	0.00	0.01	0.00	0.00	0.00	0.01	0.01	0.01	0.01	0.01	0.01
Fe^*	2.04	2.01	1.84	2.22	2.14	2.12	1.94	2.41	2.32	2.34	2.44	2.37	2.25	2.44	2.37	2.29	2.58	2.34	2.41
Mg	1.65	1.73	2.98	2.40	2.50	1.40	2.82	2.24	1.31	1.49	2.37	1.51	1.42	2.18	2.32	2.49	2.13	2.33	2.27
Mn	0.02	0.02	0.04	0.05	0.04	0.03	0.03	0.04	0.01	0.01	0.03	0.02	0.01	0.02	0.02	0.02	0.01	0.01	0.02
Ca	0.11	0.14	1.73	1.44	1.57	0.07	1.66	1.42	0.08	0.12	1.50	0.12	0.10	0.17	0.46	0.77	0.24	0.32	0.25
Na	1.91	1.90	0.28	0.73	0.50	1.94	0.34	0.71	2.01	2.00	0.64	1.96	1.96	1.90	1.66	1.31	1.82	1.76	1.81
K	0.00	0.00	0.02	0.05	0.02	0.00	0.02	0.05	0.00	0.00	0.07	0.00	0.01	0.00	0.01	0.02	0.01	0.01	0.01
Total	15.07	15.10	15.03	15.30	15.04	15.01	15.00	15.20	15.12	15.18	15.29	15.21	15.11	15.31	15.29	15.24	15.32	15.30	15.31

Notes: Calcic and sodic amphiboles were recalculated on the basis of 23 oxygens, and of 15 cations exclusive of Ca, Na and K respectively. Fe^{3+} calculated from charge balance. FeO^* = total iron.

Table 3
Epidote mineral chemistry. Representative major element compositions (wt.% oxide) and recalculated structural formulae of epidotes of metabasites from MC and CGC, and metasediments from CGC.

Unit	Morghab					Chah Gorbeh				
Sample	AK19B		AK14A			AJ33	I1309		I1311	
	Ep$_1$	Ep$_2$	Ep$_1$ (inc in Ab)	Ep$_1$	Ep$_2$	Ep	Ep (core)	Ep (rim)	Ep (core)	Ep (rim)
SiO$_2$	36.95	38.03	37.71	37.63	38.24	38.39	37.23	38.05	37.83	38.27
TiO$_2$	0.00	0.03	0.06	0.05	0.06	0.15	0.12	0.07	0.10	0.03
Al$_2$O$_3$	21.80	25.74	22.67	22.59	26.87	26.26	22.43	24.66	23.76	23.14
Cr$_2$O$_3$	0.02	0.01	0.00	0.00	0.05	0.00	0.00	0.06	0.00	0.00
FeO*	14.57	9.54	12.87	13.39	8.45	9.20	13.27	11.83	12.73	13.76
MgO	0.02	0.00	0.00	0.00	0.01	0.03	0.00	0.01	0.00	0.02
MnO	0.12	0.18	0.24	0.28	0.12	0.29	0.12	0.07	0.50	0.19
CaO	22.65	23.24	22.72	22.75	23.47	22.88	23.89	23.22	22.64	23.25
Total	96.12	96.77	96.27	96.69	97.27	97.20	97.07	97.97	97.56	98.67
Si	2.98	3.00	3.01	3.01	2.99	3.01	2.96	2.98	2.99	3.00
Ti	0.00	0.00	0.00	0.00	0.00	0.01	0.01	0.00	0.01	0.00
Al	2.07	2.39	2.14	2.13	2.48	2.43	2.10	2.28	2.21	2.13
Cr	0.00	0.00	0.00	0.00	0.00	0.00	0.00	0.00	0.00	0.00
Fe$_{2+}$	0.01	0.02	0.06	0.04	0.02	0.06	0.00	0.03	0.04	0.03
Fe$_{3+}$	0.97	0.61	0.80	0.85	0.53	0.54	0.88	0.75	0.80	0.87
Mg	0.00	0.00	0.00	0.00	0.00	0.00	0.00	0.00	0.00	0.00
Mn	0.01	0.01	0.02	0.02	0.01	0.02	0.01	0.00	0.03	0.01
Ca	1.96	1.96	1.95	1.95	1.97	1.92	2.03	1.95	1.92	1.95
Total	8.00	8.00	7.99	8.00	8.00	7.99	7.99	8.00	8.00	8.00

Notes: Structural formulae were recalculated on the basis of 8 cations. Fe^{3+} calculated from charge balance. FeO* = total iron.

2.6. Permian intrusive rocks

Several small magmatic bodies intrude the serpentinites (Torabi, 2012) cutting across their foliation. They generally consist of trondhjemites showing massive and undeformed magmatic textures.

The relative relationships between these lithologies are not always clear at the outcrop scale, although they generally postdate foliations developed in the serpentinites, often preserving primary intrusive contacts (Fig. 11).

A single U–Pb zircon age of 262 ± 1 Ma (Bagheri and Stampfli, 2008) provides a Late Permian intrusion age for them. They have been interpreted as part of a TTG suite formed by melting of a subducted basaltic crust at pressure high enough to stabilize garnet in the pre-melting assemblages (garnet amphibolite or eclogite in Torabi, 2012).

Due to their importance in the reconstruction of the evolution of the Anarak accretionary wedge, we have sampled this unit for radiometric dating of zircons.

3. Petrography, mineral chemistry and geochronology of the AMC

We focused the petrographic analysis of the rocks of the AMC on metabasites, as they are by far the most suitable rock type for the reconstruction of metamorphic evolution at HP/LT conditions. Metasediments from the Chah Gorbeh unit as well as serpentinites have been also investigated in order to provide further constraints.

Representative samples have been selected (Table 1) for: (i) detailed petrographic description, (ii) major element mineral chemistry (representative results in Tables 2–4), (iii) X-ray powder diffraction analyses on serpentinites (Table 5) and (iv) U–Pb zircon ages of a sample (AJ34) from an undeformed trondhjemite (Table 6), which intrudes the serpentinites of the Ophiolite unit (Fig. 3). Analytical techniques are described in Appendix A.

3.1. Morghab Complex

3.1.1. Metabasites

Representative samples of mafic rocks from this unit (Table 1) are porphyroblastic foliated rocks consisting of up to mm-sized albite and epidote wrapped by a fine-grained foliation defined by the orientation of chlorite + calcic-amphibole (Amp$_2$) + white mica (Wm$_2$) + titanite + epidote (Fig. 12). Albite and epidote porphyroblasts are pre-to syn-kinematic with respect to the main foliation. They preserve in their cores relics of an earlier foliation defined by the preferred orientation of titanite, glaucophane (Amp$_1$), Fe-rich epidote (Ep$_1$) and phengitic mica (Wm$_1$), while clear rims include only needles of Amp$_2$, oriented along the main foliation.

As shown in Table 2 and Fig. 13, Amp$_2$ mainly corresponds to actinolite and magnesio-katophorite. It shows a slightly zoning from core to rim, with a slight decrease in CaO, complementary to a slight increase in Na$_2$O (Table 2, Fig. 12c and f). Micron-sized Amp$_1$ included in epidote porphyroblasts is strongly enriched in Na$_2$O (7 ox. wt%, Table 2, Figs. 12c and f and 14) and corresponds to a glaucophane (Fig. 13). Amphiboles along the relict S$_1$ foliation preserved in albite do not show the same Na enrichment (Table 2, and Fig. 14) probably due to re-equilibration and cation exchange with the host albite. Also epidote shows a strong compositional variation. Particularly, Ep$_1$, included in albite porphyroblasts, shows higher Fe^{3+} contents with respect to Ep$_2$ (Table 3). Notably, Ep$_2$ is characterized by a compositional zoning (Fig. 12d) with the rim enriched in FeO* with respect to the core. This prograde zoning is likely related to the core-to-rim increase in Na$_2$O recorded by Amp$_2$.

Both white micas Wm_1 included in porphyroblastic albite and Wm_2 along the S_2 foliation show a moderate celadonitic content, in the range of 3.35–3.50 a.p.f.u. (Table 4, Fig. 15).

To summarize, Morghab metabasites record three main metamorphic events indicated by: (i) glaucophane + Ep_1 + Wm_1 + titanite (low blueschist facies) preserved along the S_1 foliation in albite and Ep_2 cores; (ii) Ab-rim + Ep_2-core + Wm_2 + Amp_2-core + chlorite (greenschist facies) developed along the main S_2 foliation; (iii) Amp_2-rim + Ep_2-rim prograde zoning indicating a pressure increase.

3.1.2. Metasediments

The Morghab metasediments chiefly consist of epidote–chlorite schist with minor quartzschist, mica schist and phyllite. The mineralogy of the epidote–chlorite schists includes abundant plagioclase with oligoclase to albitic composition, white mica and quartz. Epidote, chlorite, and minor titanite may occur (Table 1),

Table 4

Mica mineral chemistry. Representative major element compositions (wt.% oxide) and recalculated structural formulae of micas of metabasites from MC, CGC, and Ophiolite unit (metapillow), and metasediments from MC and CGC.

Unit	Morghab					Chah Gorbeh										Ophiolite unit			
Sample	AK14A				AK19B	AJ33			AK15		I1309			I1311		AK36A	AK33A		AK33B
	Wm_1	Wm_1	Wm_2 (c)	Wm_2 (r)	Wm_1	Wm_1 (cs)	Wm_2	Wm_3 (f)	Wm (f)	Wm (c)	Wm_1	Wm_2 (c)	Wm_2 (r)	Wm_1	Wm_2	Wm	Wm (cs)	Wm (f)	Wm (cs)
SiO_2	51.89	51.83	53.59	51.99	52.27	51.18	52.25	52.17	51.85	52.06	51.74	51.33	51.11	51.44	51.30	54.51	53.35	54.32	54.14
TiO_2	0.07	0.10	0.00	0.24	0.05	0.11	0.12	0.12	0.30	0.38	0.36	0.34	0.13	0.39	0.33	0.09	0.03	0.09	0.05
Al_2O_3	29.74	26.34	27.40	25.36	28.77	26.88	28.34	28.84	29.49	29.35	25.27	27.79	28.42	26.82	27.94	24.81	25.44	25.28	24.54
Cr_2O_3	0.00	0.00	0.03	0.00	0.08	0.00	0.01	0.08	0.02	0.00	0.05	0.10	0.00	0.05	0.00	0.16	0.19	0.08	0.08
FeO^*	3.76	4.28	3.42	6.50	3.38	4.99	4.26	3.58	3.39	3.23	6.96	5.76	5.30	6.20	5.59	3.95	4.49	4.65	4.08
MgO	1.91	4.40	3.10	3.06	2.53	2.32	2.19	2.50	2.23	2.45	3.00	2.30	2.07	2.63	2.20	3.79	3.41	3.54	3.91
MnO	0.04	0.00	0.00	0.00	0.01	0.03	0.06	0.06	0.01	0.04	0.02	0.00	0.04	0.00	0.02	0.00	0.01	0.01	0.03
CaO	0.04	0.19	0.08	0.07	0.00	0.01	0.00	0.01	0.00	0.00	0.04	0.00	0.00	0.13	0.02	0.00	0.03	0.02	0.01
Na_2O	0.27	0.23	0.21	0.13	0.33	0.19	0.25	0.23	0.34	0.11	0.07	0.34	0.44	0.42	0.33	0.10	0.16	0.07	0.07
K_2O	9.64	9.19	10.08	9.48	9.84	9.55	9.45	9.70	9.49	9.78	10.37	9.65	9.59	9.47	9.88	9.97	10.19	8.94	10.16
Total	97.37	96.56	97.90	96.83	97.27	95.25	96.93	97.29	97.12	97.40	97.88	97.61	97.10	97.55	97.61	97.38	97.30	97.00	97.06
Si	3.38	3.42	3.47	3.46	3.41	3.43	3.42	3.40	3.38	3.38	3.43	3.38	3.37	3.40	3.38	3.56	3.50	3.55	3.55
Ti	0.00	0.00	0.00	0.01	0.00	0.01	0.01	0.01	0.01	0.02	0.02	0.02	0.01	0.02	0.02	0.00	0.00	0.00	0.00
Al	2.28	2.05	2.09	1.99	2.21	2.13	2.19	2.22	2.26	2.25	1.98	2.16	2.21	2.09	2.17	1.91	1.97	1.94	1.90
Cr	0.00	0.00	0.00	0.00	0.00	0.00	0.00	0.00	0.00	0.00	0.00	0.01	0.00	0.00	0.00	0.01	0.01	0.00	0.00
Fe^*	0.20	0.24	0.19	0.36	0.18	0.28	0.23	0.20	0.18	0.18	0.39	0.32	0.29	0.34	0.31	0.22	0.25	0.25	0.22
Mg	0.19	0.43	0.30	0.30	0.25	0.23	0.21	0.24	0.22	0.24	0.30	0.23	0.20	0.26	0.22	0.37	0.33	0.34	0.38
Mn	0.00	0.00	0.00	0.00	0.00	0.00	0.00	0.00	0.00	0.00	0.00	0.00	0.00	0.00	0.00	0.00	0.00	0.00	0.00
Ca	0.00	0.01	0.01	0.01	0.00	0.00	0.00	0.00	0.00	0.00	0.00	0.00	0.00	0.01	0.00	0.00	0.00	0.00	0.00
Na	0.03	0.03	0.03	0.02	0.04	0.02	0.03	0.03	0.04	0.01	0.01	0.04	0.06	0.05	0.04	0.01	0.02	0.01	0.01
K	0.80	0.77	0.83	0.80	0.82	0.82	0.79	0.81	0.79	0.81	0.88	0.81	0.81	0.80	0.83	0.83	0.85	0.74	0.85
Total	6.89	6.95	6.91	6.95	6.91	6.92	6.89	6.90	6.89	6.89	7.00	6.95	6.95	6.97	6.96	6.90	6.94	6.85	6.92

Notes: Structural formulae were recalculated on the basis of 11 oxygens and 2(OH), all Fe^{2+}. FeO^* = total iron. Abbreviations – c: core; r: rim; cs: coarse; f: fine.

Table 5
XRPD data. Mineralogical composition of the studied serpentinites as detected by XRPD analyses.

Sample	AK31	AK44	I13-38	I13-52	I13-55	I13-56	I13-63
Serpentine	++	++*	++	++*	++	++	++*
Chlorite				O	+	+	
Magnetite	+	+	+	+	+	+	+
Olivine							O
Clinopyroxene	O		O				
Talc				+			
Carbonates	O			O		O	

Notes: (++) major phase (>10 wt.%), (+) minor phase (<10 wt.%), (O) phase in trace amounts, and () below detection limit (<1 wt.%). The asterisk indicates the presence of antigorite.

together with minor Fe–Ti oxides, apatite and rare zircon. Quartzschist and mica schist consist of quartz, albite, white mica and chlorite. Biotite occurs together with garnet in samples with metapelitic compositions, collected at the northern margin of the unit (SW of Chah Karbuzeh, Fig. 3).

All the studied samples have S-tectonite textures with the main foliation (S_2) defined by mineral assemblages typical of greenschist facies conditions (Wm_2 + Chl + Qtz), both in epidote–chlorite schist and in metapelites.

The occurrence of a pre-existing foliation (S_1), supposed on the basis of field evidence, is confirmed at the microscale, where preto syn-S_2 albite and epidote porphyroblasts frequently preserve an internal foliation that in some cases is disposed at high angle with the external S_2, or evenly folded (Fig. 16). The foliation preserved in epidote is marked by trails of micrometric inclusions of white mica (Wm_1), quartz, Fe–Ti oxides and plagioclase.

In mica schists S_2 is marked by the shape preferred orientation of white mica (Wm_2) and biotite (Bt_1), which is often almost completely substituted by chlorite. Pre-S_2 likely aligned white mica relics (Wm_1), often define an older foliation (S_1). Albite occurs as pre- to syn-S_2 porphyroblast. Garnet occurs only in samples with strictly pelitic composition collected at the northern margin of the Morghab unit (Table 1). Garnet forms pre-S_2 porphyroblast, up to a few millimeters in size, in equilibrium with Bt_1 in their strain shadow. Two generations of biotite occur in garnet-bearing samples. The second one (Bt_2) grows together with white mica (Wm_2) along the regional foliation (S_2).

3.2. Chah Gorbeh Complex

3.2.1. Metabasites

Representative samples of mafic rocks from this unit (Table 1) are characterized by albite and epidote porphyroblasts, preserving a S_1 foliation given by titanite, albite, quartz and actinolitic hornblende (Amp_1), along a foliation given by quartz ribbons, chlorite, white mica, magnetite and alkali-amphibole (Fig. 17a). Exception done for rare actinolitic amphiboles, alkali-amphiboles characterizing the main foliation show homogeneous compositions with the highest Na_2O contents (>7 wt%, Table 2) and are classified as Ferro-glaucophane (Fig. 13). In a Na/(Na + Ca) versus Al((Si + Al) diagram (Fig. 14) they show a trend similar to that of amphiboles from Morghab Complex with the difference that this is prograde, with Na enrichment from Amp_1 to Amp_2. In addition, Amp_2 from Chah Gorbeh metabasites are even more enriched in Na with respect to Ca, compared with Amp_1 included in epidote from Morghab mafic rocks (Fig. 14a and b). Glc from Chah Gorbeh is syn- to post-kynematic with respect to the S_2 foliation. This is evidenced by clear cores (exception done for calcite inclusions) compared with inclusion-rich rims. Such inclusions consist of the same mineral phases as those crystallized along the main foliation (Chl, Ab, Wm, Ep and rutile with Tit coronas; Fig. 17c). In some samples also epidote along the S_2 foliation shows a poikiloblastic texture and includes quartz, albite and titanite. Such epidotes are Fe^{3+} enriched, in agreement with equilibration with glaucophane (Table 3).

From the petrographic analyses and mineral chemistry, the mafic rocks from Chah Gorbeh Complex show: (i) a relict Ep + Ab + Tit + Amp_1 greenschist facies paragenesis (S_1) preserved in the cores of epidote and albite porphyroblasts; (ii) main Chl + Glc + Fe-Ep + Ab + Mt + Wm paragenesis syn-to-post-S_2 (low blueschist facies conditions). The absence of a mineral zoning in glaucophane suggests that such mineral association did not record retrocession during its evolutionary history.

Samples of silicate-bearing marbles were collected at the northern contact with one of the largest serpentinite thrust sheet (Site Ir4, Fig. 4 and Table 1). They show a peculiar mineral assemblage characterized by an intergrowth of carbonate and silicate mineral phases. Interestingly, they show post-kinematic prismatic glaucophane (Fig. 17b, d and e). In these carbonate rocks magnetite also occurs (Fig. 17f), together with crystals of spinel, suggesting a metasomatic interaction with the adjoining serpentinites. The occurrence of both glaucophane in the marbles and of antigorite in the serpentinites (see Section 3.4) suggests a common HP equilibration of the two lithologies.

3.2.2. Metasediments

Metasediments of the Chah Gorbeh Complex consist of mica schist, epidote-bearing gneiss and greenschist. Thin layers of carbonate-bearing schists occur along the contacts of the numerous marble lenses that represent a peculiar lithological feature of this unit.

Epidote–chlorite schist and gneiss are the most common lithologies and they closely resemble the ones of the Morghab unit, except for the occurrence of stilpnomelane, biotite and rare titanite (Table 1) in Chah Gorbeh samples. Amphibole is rare.

Within the epidote gneiss, the main foliation S_2 is marked by the preferred orientation of Wm_2 + Chl + Qtz + Pl_2. A typical microstructural feature is the occurrence of pre-S_2 plagioclase (Pl_1) porphyroblasts preserving relics of an older foliation (S_1) as inclusions trails. The S_1 within plagioclase consists of white mica (Wm_1), epidote

(Ep_1) and Fe–Ti oxides. Titanite and garnet (Grt_1) also occur as inclusions within plagioclase (Fig. 18c–f). In the matrix, the S_1 relics are represented by partly retrogressed biotite (Bt_1) and white mica (Wm_1).

The second generation of plagioclase (Pl_2) is albite and occurs both along the S_2 foliation and as thin rims on Pl_1 porphyroblasts. In few samples (e.g. AJ33, Fig. 18), also a second generation of Mnrich garnet (Grt_2) and epidote (Ep_2) grow within the mica-rich domains of the S_2 foliation.

A typical feature is the occurrence of radiate aggregates of stilpnomelane (Stp_1) growing statically on the S_2 foliation (Fig. 19), postdating the main tectonometamorphic phase (D_2).

A third deformation phase (D_3) is also recorded at the microscale. A new axial plane foliation develops in some samples either marked by a second generation of stilpnomelane (Stp_2) or a third generation of fine-grained white mica (Wm_3).

Electron microprobe analyses (EMPA) show that both Wm_1 and Wm_2 have a phengitic composition, with Si ranging between 3.4 and 3.5 a.p.f.u. and a (K/Na + K) ratio of 0.95–0.99 (Table 4, Figs. 15 and 20). Such compositions point to relatively HP/LT in agreement with the metamorphic evolution determined for the metabasites of both CGC and MC. In sample AJ33, the third generation of mica (Wm_3) displays a celadonitic component (Fig. 15), slightly lower than Wm_1 and Wm_2, in general agreement with the occurrence of stilpnomelane postdating D_2 phase in the other studied samples.

Table 6
U–Pb dating. SHRIMP U–Pb analytical data performed on zircons separated from sample AJ34.

Spot	$^{206}Pb_c$ (%)	U (ppm)	Th (ppm)	$^{232}Th/^{238}U$	$^{206}Pb^*$ (ppm)	^{204}Pb-corrected							Apparent age	
						Ratios								
						$^{207*206}Pb/Pb$	±1r (%)	$^{207*235}Pb/U$	±1r (%)	$^{206*238}Pb/U$	±1r (%)	Err. corr.	$^{206\ 238}Pb/U$ (Ma)	±1r (abs.)
AJ34-1 c	0.33	299	442	1.53	25.0	.0585	2.2	0.78	2.3	.0967	0.6	.265	595.2	±3.4
AJ34-2 c*	0.97	140	190	1.40	12.8	.0551	5.2	0.80	5.3	.1054	1.0	.189	646.0	±6.2
AJ34-3 c	0.49	236	126	0.55	19.1	.0571	2.9	0.74	2.9	.0936	0.6	.210	577.0	±3.4
AJ34-4 c	0.84	68	145	2.20	5.5	.0606	7.7	0.78	7.8	.0935	0.8	.102	576.2	±4.4
AJ34-5 r*	0.24	121	39	0.33	45.0	.1762	0.8	10.45	1.1	.4303	0.8	.738	2307.1	±16
AJ34-6 r	0.91	435	126	0.30	17.5	.0520	4.1	0.33	4.2	.0463	0.6	.150	292.0	±1.8
AJ34-7 c**	2.41	48	101	2.18	3.9	.0542	14.3	0.68	14.4	.0914	1.8	.123	564.1	±9.6
AJ34-8 r	0.35	307	125	0.42	20.5	.0546	3.0	0.58	3.0	.0776	0.7	.214	481.6	±3
AJ34-9 r	0.64	140	65	0.48	14.0	.0621	4.2	0.99	4.3	.1152	0.9	.213	702.7	±6.1
AJ34-10 r	0.96	316	105	0.34	12.7	.0523	3.7	0.33	3.8	.0462	0.7	.194	291.1	±2.2
AJ34-11 r	1.40	62	37	0.62	8.6	.0668	7.0	1.47	7.0	.1594	0.9	.131	953.6	±8.2
AJ34-12 r	0.58	299	71	0.25	19.0	.0586	3.2	0.59	3.2	.0735	0.7	.213	457.1	±3
AJ34-13 r	0.76	265	96	0.37	10.4	.0520	3.5	0.33	3.6	.0463	0.8	.219	291.9	±2.2
AJ34-14 r	0.06	1099	181	0.17	102.1	.0606	0.8	0.90	0.8	.1080	0.4	.422	661.3	±2.3
AJ34-15 r	0.38	119	73	0.64	10.4	.0627	3.9	0.88	4.1	.1012	0.9	.231	621.7	±5.6
AJ34-16 c*	0.03	856	32	0.04	295.7	.1444	1.5	8.00	1.5	.4020	0.4	.232	2178.5	±6.5
AJ34-17 c	0.33	239	152	0.66	21.6	.0590	2.5	0.85	2.6	.1048	0.7	.258	642.6	±4.1
AJ34-18 r	0.81	294	119	0.42	12.0	.0519	3.5	0.33	3.6	.0463	0.7	.209	291.6	±2.2
AJ34-19 r	0.23	428	139	0.34	16.2	.0523	2.4	0.33	2.4	.0459	0.6	.266	289.4	±1.8
AJ34-20 r*	5.54	527	70	0.14	35.2	.0509	10.4	0.52	10.5	.0734	1.0	.094	456.6	±4.3
AJ34-21 r	0.18	488	113	0.24	32.3	.0557	1.7	0.59	1.7	.0771	0.5	.273	478.8	±2.2

Notes: Errors are 1-sigma; Pb_c and Pb^* indicate the common and radiogenic portions, respectively. Common Pb corrected using measured ^{204}Pb. Error in Standard calibration was 0.16% (not included in above errors but required when comparing data from different mounts). c: core; r: rim. Discarded spots in italic: *discordant analyses due to suspected Pb loss, **high common $^{206}Pb_c$ portion.
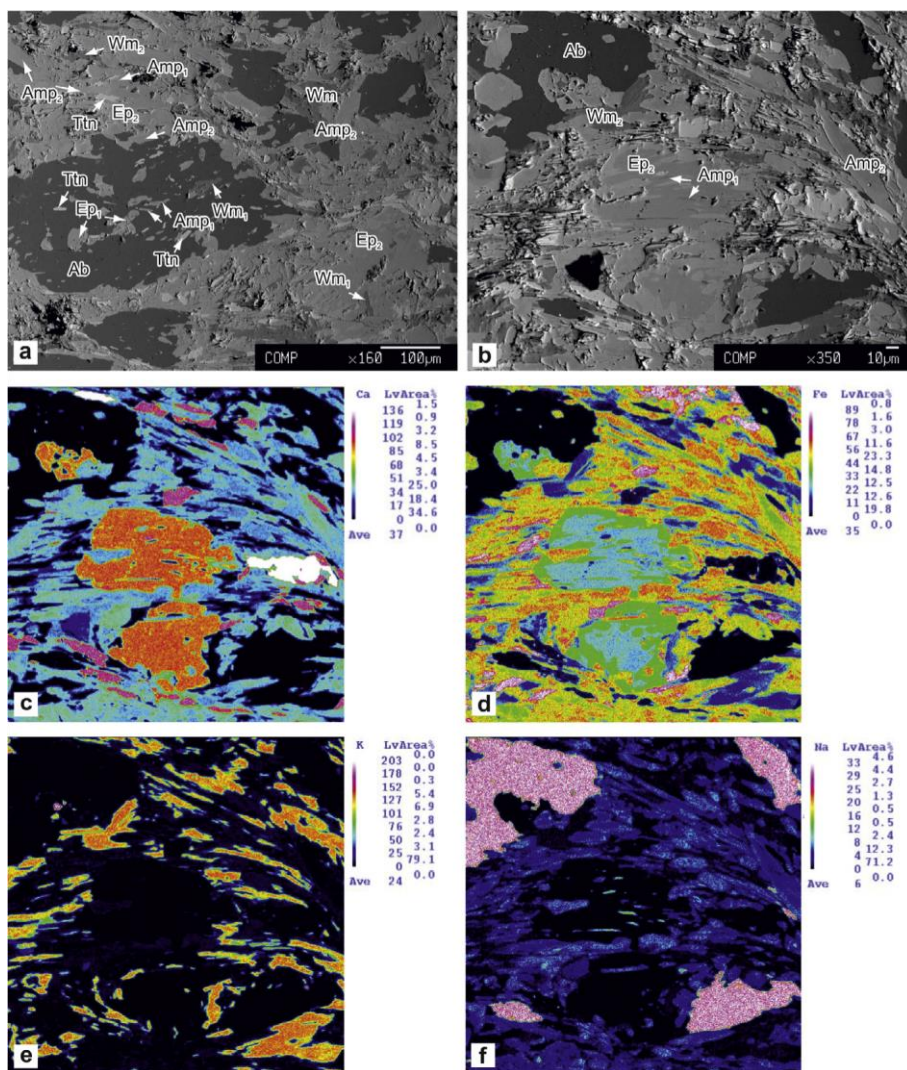
Fig. 12. BSE images (a and b) and X-ray elemental maps (c–f) of representative microstructures of metabasite AK14A from the Morghab Complex. (a and b) Albite (Ab) and epidote (Ep_2) porphyroblasts enveloped by the main foliation given by calcic- and sodic-calcic-amphibole (Amp_2), white mica (Wm_2) and titanite (Ttn). Relict S_1 foliation is preserved inside the porphyroblasts and is marked by inclusions of Ttn, Fe-rich epidote (Ep_1), white mica (Wm_1) and actinolitic amphibole (Amp_1) in Ab, and inclusions of Ferich epidote (Ep_1) and glaucophane (Amp_1) in Ep_2. (c–f) Ca, Fe, K, Na elemental maps of glaucophane and Fe-rich epidote inclusions in Ep_2.

3.3. Ultramafic rocks

According to Wicks and O'Hanley (1988), most of the serpentinite samples show interpenetrating and interlocking non-pseudomorphic textures, occasionally with poorly preserved bastites (samples AK31, AK44, I13-38 and I13-52, see Table 1). Chrysotile occurs in some samples, infilling late-stage cracks and micro-fractures that formed after the main tectonometamorphic phase (D_2).

Serpentinites are folded together with the CGC within the D_2 fold system; their foliation follows the regional S_2 trend and it is refolded by subsequent events (Figs. 3, 4, 6 and 7).

Due to the uneasy identification of serpentinite polymorphs under the optical microscope, we performed X-ray diffractometer analyses to characterize the mineralogy of the studied samples (Table 5).

The occurrence of antigorite coexisting with lizardite (Fig. 21) in three selected analyzed samples indicates that the metamorphic peak conditions in the serpentinites unit is similar to that determined from the blueschist facies assemblages of Chah Gorbeh, Morghab and meta-pillow lavas unit.

At P > 9 Kbar, antigorite is stable together with lizardite in the 320–390 C temperature range, as determined by field studies of serpentinites preserved within accretionary wedges (e.g. Schwartz et al., 2013). Above 400 C, lizardite is not stable and is completely substituted by antigorite. At low to mild pressure, the upper temperature stability of antigorite is determined by the formation of secondary olivine at T 450 C (Evans, 2004). Existing data suggest also that antigorite stability is not only temperature dependent, but also pressure dependent (Ulmer and Trommsdorff, 1995; Wunder and Schreyer, 1997). These results are in general agreement with the absence of antigorite in serpentintes at T < 300 C and P < 4 Kbar (Schwartz et al., 2013).

The above considerations, together with field structural data, indicate that the Anarak serpentinites were subducted and later exhumed together with the CGC and MC.

3.4. Meta-pillow basalts

The meta-pillow basalts show a very weak foliation given by albite, chlorite, white mica, actinolitic amphibole, epidote and titanite. Prismatic alkali-amphibole, coarse magnetite and a second generation of titanite statically overgrow the main greenschist paragenesis (Fig. 22). Locally, alkali-amphibole may form coronas around albite and chlorite + actinolitic amphibole sites.
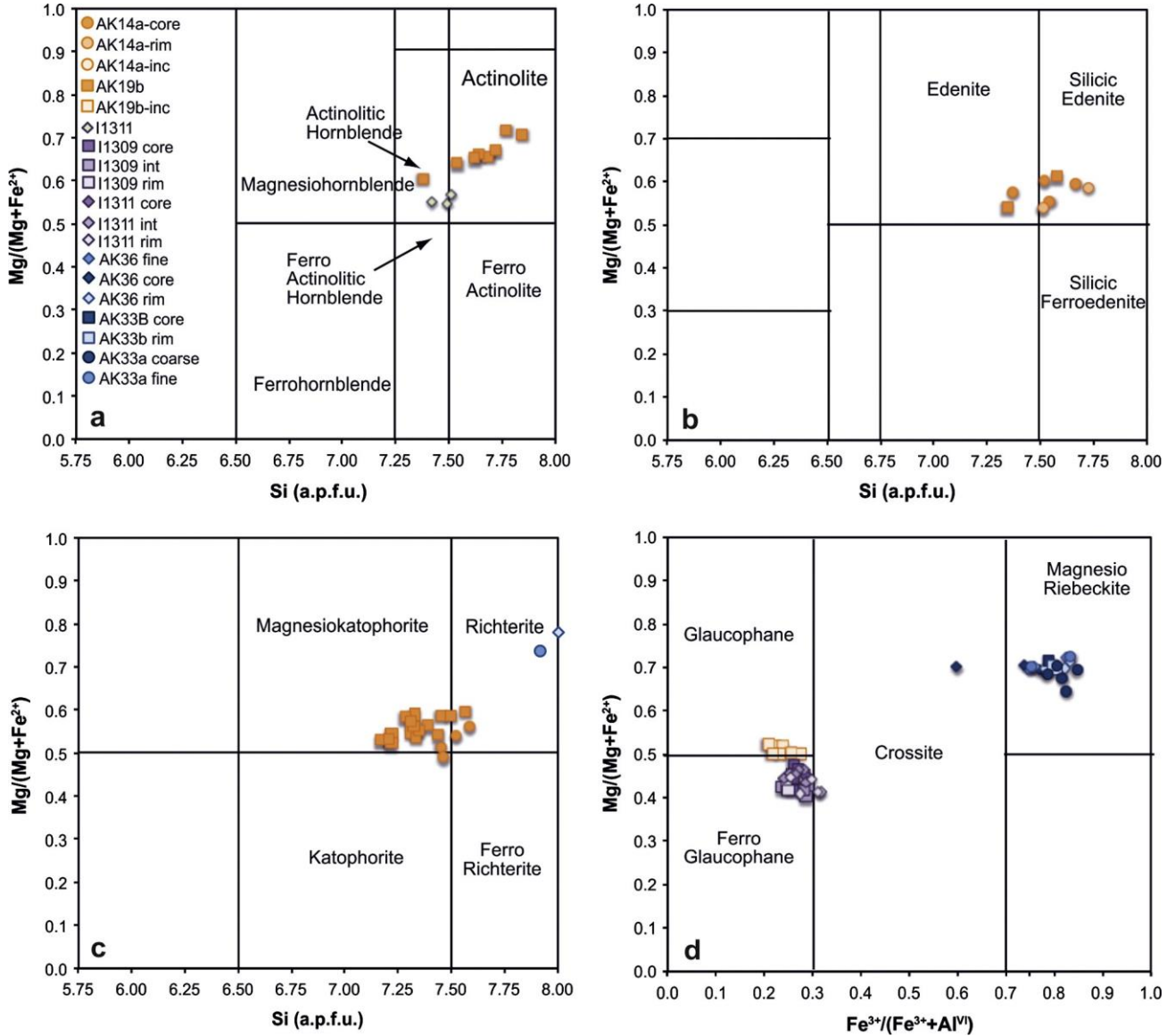

Fig. 13. Composition of amphiboles from the studied selected samples plotted in the Si and $Fe^{3+}/(Fe^{3+}+Al^{VI})$ versus $Mg/(Mg + Fe^{2+})$ atoms per formula unit (a.p.f.u.) diagrams (Leake et al., 1997).
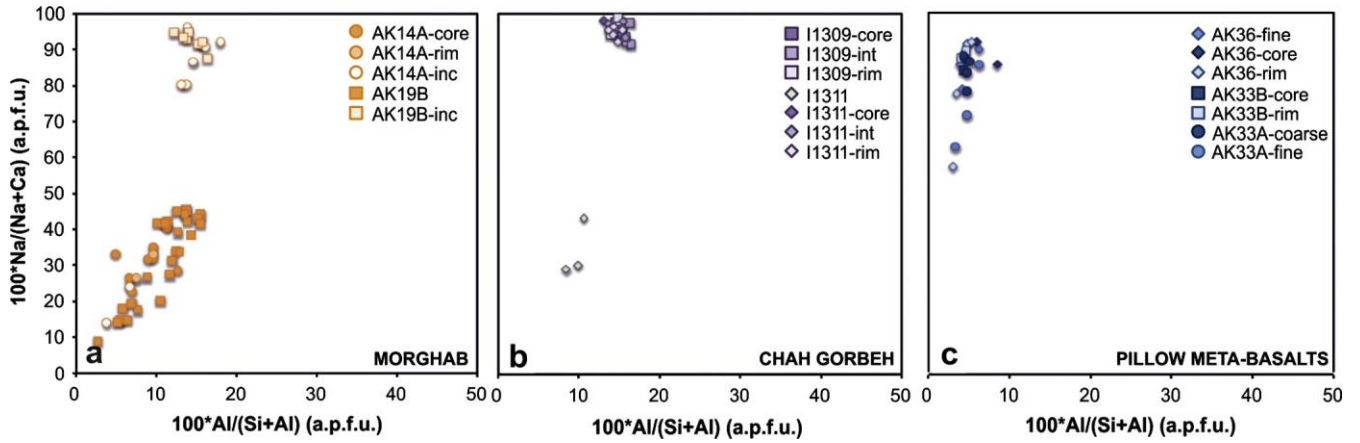
Fig. 14. Compositions of calcic, sodic–calcic and alkali amphiboles from the Morghab Complex (a), Chah Gorbeh Complex (b) and meta-pillow (c) in the 100Na/(Ca + Na) versus 100Al/(Si + Al) diagram.
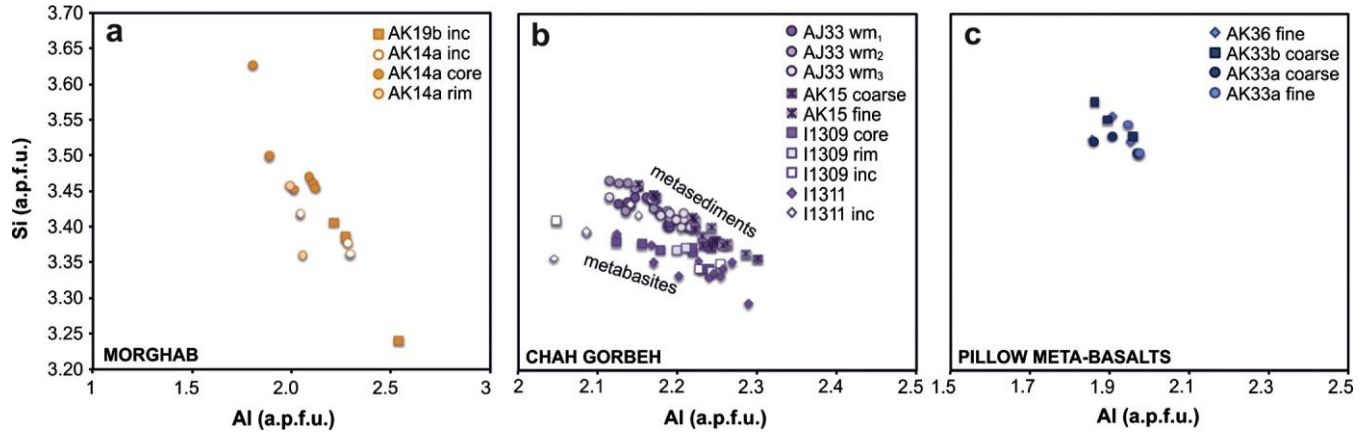

Fig. 15. Compositions of phengitic micas in the Al versus Si diagram from Morghab Complex (a), Chah Gorbeh Complex (b) and meta-pillows (c).
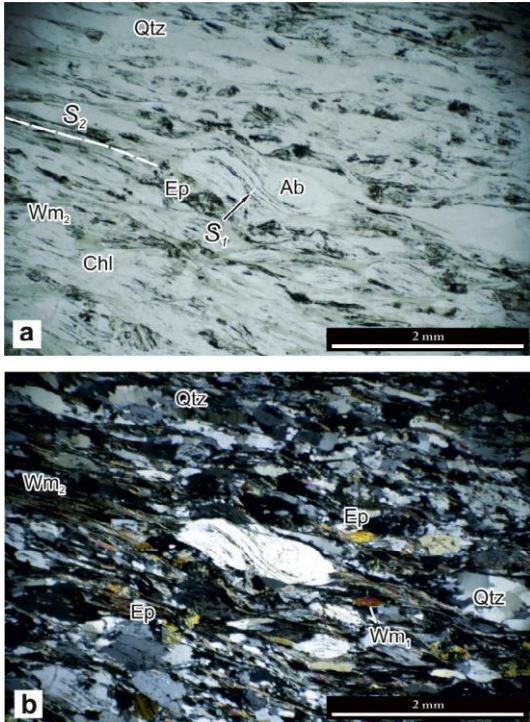

Fig. 16. Photomicrographs (transmitted light) of the MC rocks. (a) Plagioclase porphyroblasts in epidote–chlorite schist. Plagioclase is pre- to early-S_2 and preserves an internal foliation made of aligned inclusions of Qtz, Wm, Ep and oxides. (b) Crossed-polarized image of (a).

Alkali-amphibole is homogeneous in composition and corresponds to a Mg-riebeckite. It shows slightly lower Na content with respect to alkali-amphibole occurring in the Chah Gorbeh mafic rocks (Table 2, Fig. 14b and c). Some coarse white micas appear in textural equilibrium with riebeckite (Fig. 22a). However, the relationship between possible two mica generations and the other mineral phases are not clear due to the very weak foliation characterizing the analyzed samples. This is also confirmed by the homogeneous composition shown by coarse and fine-grained micas (Fig. 15c), characterized by a moderate celadonitic substitution. The celadonitic content is, however, the highest (Si up to 3.56 p.f.u., Table 4) compared with white micas of mafic rocks from the CGC and MC (Figs. 15 and 20). This comparison suggests that phengitic micas of meta-pillow basalts likely re-equilibrated with riebeckite under blueschist facies conditions during a prograde, relatively HP, metamorphism.

3.5. Permian intrusive rocks

Trondhjemites intruded the accretionary wedge of Anarak in different sectors (Torabi, 2012), being concentrated in an E–W trending zone comprised between Darreh Anjir mountains to SW and Chah Gorbeh mountains to NE (Fig. 2). We reported in our geological maps (Fig. 3) only the main bodies.

The origin and geodynamic significance of such rocks is beyond the aim of the paper, but in the frame of this work, they are of paramount importance as they can help to determine a minimum age for the metamorphism of the Anarak wedge. Bagheri and Stampfli (2008) obtained a Late Permian age (262.3 ± 1.0 Ma) for a trondhjemite stock located SE of Chah Derakhtak.

We processed several samples, but only one of these (AJ34, Table 1 and Fig. 3) yielded enough zircons for U–Pb dating. SHRIMP U–Pb analyses of zircons from sample AJ34 provided a complex Neoproterozoic to Palaeozoic age distribution (Fig. 23a) due to the occurrence of abundant xenocrysts. Four spots are discordant (Table 6) and then discarded from discussion. The remaining sixteen analyses span over a large range of concordant and nearly concordant ages from 953.6 ± 8.2 to 289.4 ± 1.8 Ma (Fig. 23b and c).

The spot analyses from 953.6 ± 8.2 to 456.6 ± 4.3 Ma were performed on both rims and cores. They can be roughly grouped into clusters of Tonian (953.6 ± 8.2), Cryogenian (three spots: 702.7 ± 6.1 to 642.6 ± 4.1), Ediacaran (four spots: 621.7 ± 5.6 to 576.2 ± 4.4), Early (481.6 ± 3 and 478.8 ± 2.2) and Late Ordovician (457.1 ± 3) ages (Fig. 23a). Five younger analyses performed on rims (Fig. 23d) gave an Early Permian age (five spots: 292 ± 1.8 to 289.4 ± 1.8; Table 6) with a weighted average $^{206}Pb/^{238}U$ mean age of 291.1 ± 1.8 Ma (2r; MSWD = Mean Square of Weighted Deviates = 0.3, Prob. = Probability of fit = 0.9; Fig. 23b and c). We tentatively interpret this latter age as the crystallization age of the AJ34 trondhjemite dike. Age distribution of the dated sample is similar to U–Pb ages obtained in the Gondwanan domain all over Iran and in the eastern Mediterranean (Horton et al., 2008; Kydonakis et al., 2014; Rossetti et al., this vol.), indicating a possible contamination from portions of a Gondwana-related crust.

4.   Structural and metamorphic history of the AnarakMetamorphic Complex wedge

4.1. Late Palaeozoic structural evolution of the Anarak accretionary wedge

Based on field evidence, and on microstructural analyses, the MC and CGC display a partially common deformation history, in which we recognized at least three major deformational events.
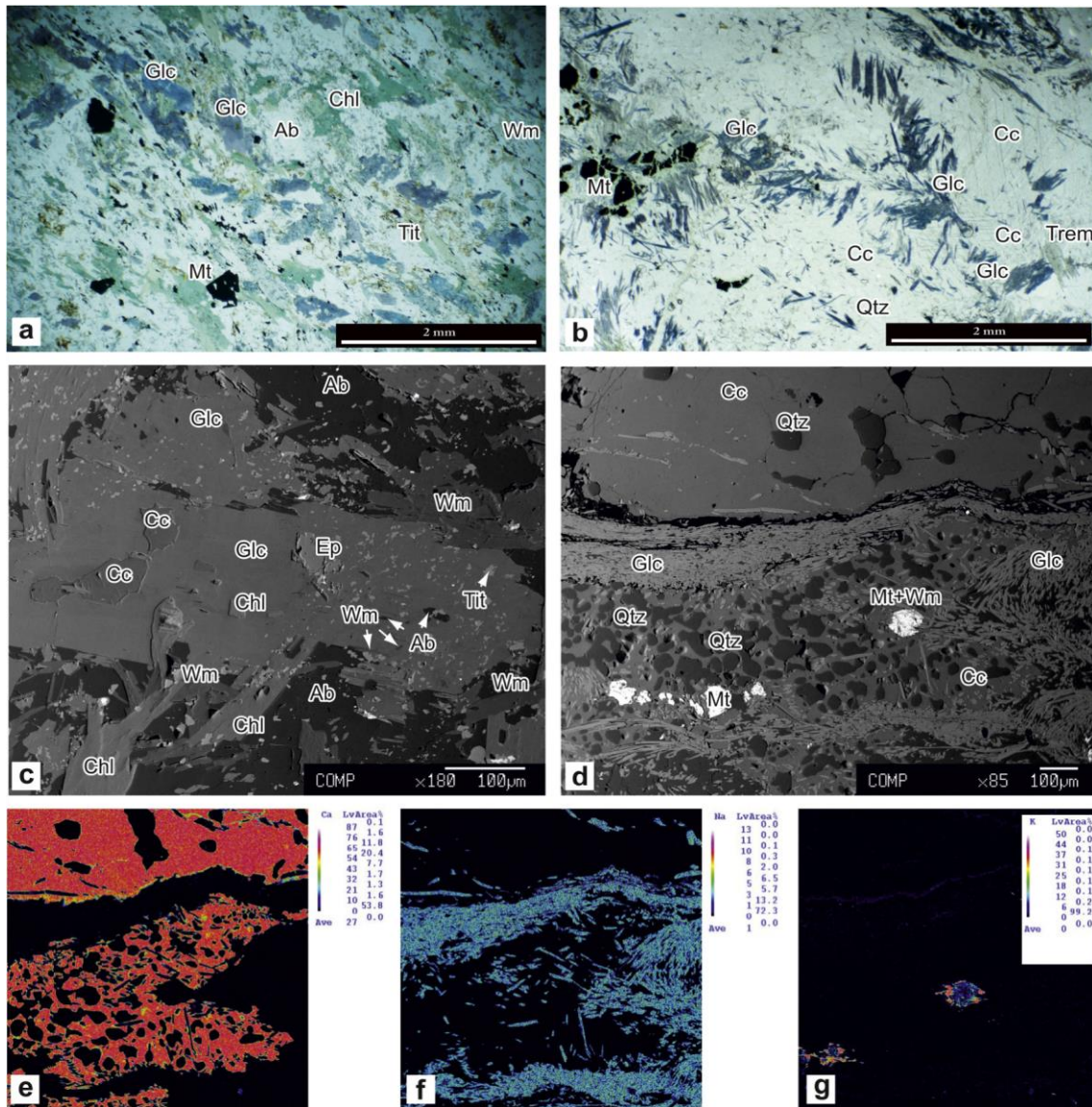
Fig. 17. Photomicrographs (transmitted light and BSE images) of representative rock-forming minerals of metabasites I13-09 and I13-11, and metacarbonate I13-37 from the Chah Gorbeh Complex. (a) Magnetite (Mt) and glaucophane (Glc) poikiloblasts grow along the main foliation defined by white mica (Wm), chlorite (Chl), albite (Ab) and titanite (Ttn). (b) syn- to post-kinematic glaucophane showing rims enriched by inclusions of the main foliation mineral phases. Note inclusions of calcite (Cc) within the core. (c) Magnetite porphyroblasts, glaucophane and rare tremolite (Trem) statically overgrow the main foliation defined by calcite and quartz (Qz) in silicate marbles (Fig. 2 and Table 1 for sample location). (d–g) BSE image and X-ray Ca, Na. K elemental maps of glaucophane in silicate marbles
.

A first stage (D$_1$) is recognizable in both units. It was characterized by the formation of isoclinal folds associated with a pervasive axial plane foliation causing a complete transposition of the primary stratigraphic characters. These foliations record different metamorphic conditions in the two units, as previously described: (i) blueschists facies in the MC, and (ii) slightly higher T and/or lower P in the CGC.

Isoclinal folds related to a subsequent D$_2$ deformational stage, with axes varying from sub-horizontal to vertical, superposed on the S$_1$ foliation, clearly outcrop in these two units especially in the area north of Kuh-e Chah Gorbeh. This fold system shows the same style, continuous across the two units, and developed in similar metamorphic conditions in both units. We therefore suggest that the two units coupled before or at least during the D$_2$ event.

Most of the contacts between the CGC lithologies and the serpentinites often show a strong brittle reactivation due to competence contrasts. However, we could observe some preserved original relationships along the watershed between the Mileh and Chah Gorbeh basins, where serpentinites are deeply involved in the D$_2$ folds (Figs. 3, 4 and 6). In addition, along the contact with serpentinites, where mylonitic fabrics are often present in the CGC, the D$_2$ foliation shows the growth of glaucophane, suggesting that coupling and folding of the two units occurred during a prograde metamorphism under blueschist facies conditions.

A similar structural evolution is also evident in the MC south of Anarak around Kuh-e Pol-e-Khavand, where also felsic meta-volcanic rocks occur. Isoclinal intrafolial folds can be ascribed to a D$_1$ deformational event generating the S$_1$ axial plane schistosity. This was refolded by a second D$_2$ pervasive event forming tight to isoclinal folds. A diffused crenulation cleavage formed at greenschist facies conditions during this second event.

Greenschist facies ductile shear zones deform the blueschist meta-pillows and are overprinted by the growth of riebeckite, therefore recording a well-preserved prograde evolution. Such evolution can be compared with the one recorded in the CGC and can be tentatively correlated with the pre-D$_3$ evolution of the
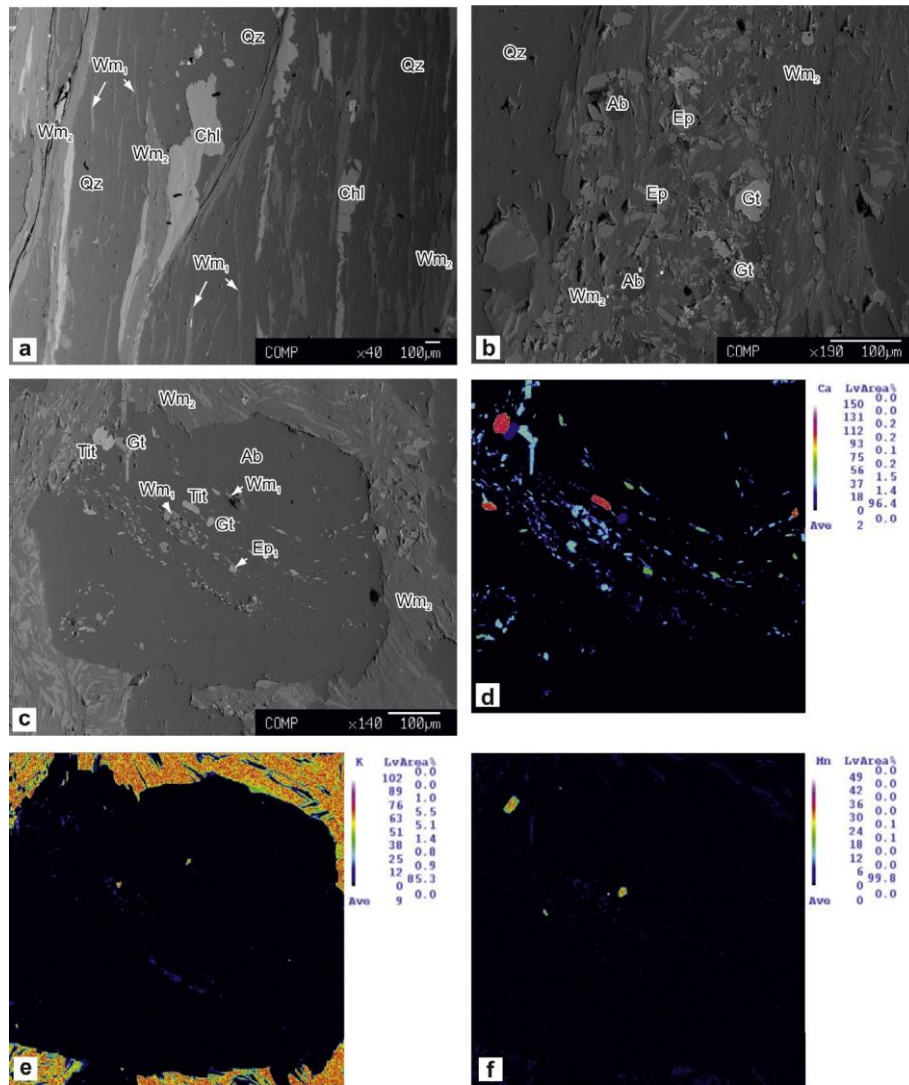
Fig. 18. BSE images (a–c) and X-ray Ca, K, Mn elemental maps (d–f) of representative microstructures of metasediments (samples AK15 and AJ33, Table 1 and Fig. 2) from the Chah Gorbeh Complex. (a) Relict S_1 foliation in sample of micaschist AK15 is marked by fine-grained white mica (Wm$_1$), whereas the main foliation (S_2) is marked by coarser white mica (Wm$_2$), chlorite (Chl) and quartz (Qz). (b) S_2 foliation in sample AJ33 is marked by white mica, albite, titanite, epidote, quartz and Mn-rich garnet (Gt). (c–f) S_1 folded relict foliation preserved in albite porphyroblast marked by oriented inclusions of white mica (Wm$_1$), epidote, titanite and garnet.

accretionary wedge. Here the static growth of calcic-sodic amphibole with a lower Na content also follows dynamic recrystallization along South-verging shear zones.

Semi-brittle to brittle fault zones with ophicalcite tectonic breccias occur at the base of these exposures within the serpentinites, as well as along the contacts between the CGC and serpentinites, recording a transition to brittle conditions (Fig. 9). Fault planes and ductile shear zones suggest a dominant S- to SSE-verging tectonic transport both for ductile and brittle structures.

Variable trend and plunge of the D_2 folds are related to a third important D_3 large scale folding event, superposed on previous structures. A spectacular interference pattern between the D_1/D_2 and D_3 fold systems outcrops to the east of Kuh-e Chah Gorbeh. Large scale superposed folds are evident in the area dominated by the high carbonate peaks formed by isoclinally folded layers belonging to the CGC. D_2 isoclinal folds traced by thick marble layers are refolded by impressive upright strongly plunging to vertical folds (''schlingen'' in Alpine literature) due to a D_3 folding stage.

The D_3 fold systems affect both the CGC and the MC. The same deformation also affected the serpentinite slivers, tectonically incorporated in the lower part of the CGC during the D_2 deformation, and possibly part of the Lakh Marble thrust sheet.

Mesoscopic observations from the area between Mileh and Chah Gorbeh (Figs. 4 and 7) indicate the complexity of the geometrical features resulting by the superposition of the two folding events. The S_2 foliation is generally vertical, whereas the plunge of D_2 fold axes is strongly variable ranging from horizontal to sub-vertical, depending on their position with respect to the D_3 hinge zones. Folding of the S_2 foliation and D_2 axial surfaces is evident at site AN12 (Fig. 4, Mileh mine), as suggested by the dispersion of poles to the S_2. D_3 folds are open to close with a variable generally steep plunge. The hinge style of the D_3 fold varies from concentric to angular (Fig. 7b and c) and no pervasive axial plane foliations developed during this stage. A view of the interference pattern exposed in the nose of the main D_3 antiform of Mileh is shown in Fig. 7a. D_3 folds with variable wavelengths occur everywhere in the Anarak area and show steeply plunging to vertical axes (Fig. 4).

A map of the metamorphic foliation has been obtained from Google Earth (Fig. 4). D_2 isoclinal folds are clearly distinguished in the map along thickened marble layers. D_2 foliations were also
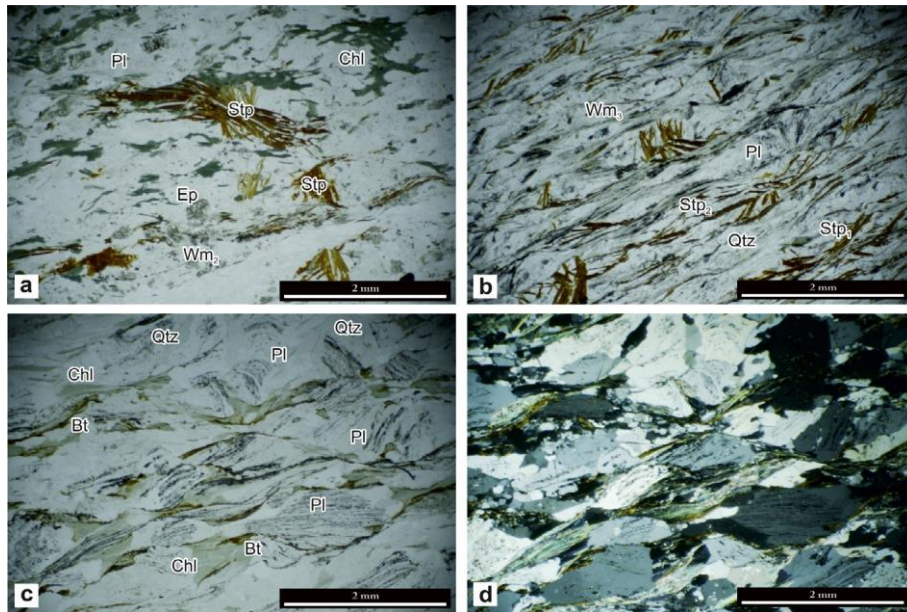
Fig. 19. Photomicrographs (transmitted light) of the CGC metasediments. (a) Stilpnomelane statically overgrown on the S$_2$ foliation marked by the shape preferred orientation of Wm$_2$ and Chl (sample AJ13). (b) A second generation of stilpnomelane growths along a mylonitic foliation within a secondary shear zone close to the contact between CGC and MC (sample AJ14). (c) Pre-S$_2$ plagioclase porphyroblasts preserve inclusion trails (Qtz + Chl + Wm$_1$ + oxides) defining an internal foliation (S$_1$) at high angle with respect to S$_2$. Chlorite replace biotite along the main foliation. (d) Crossed-polarized image of (c).
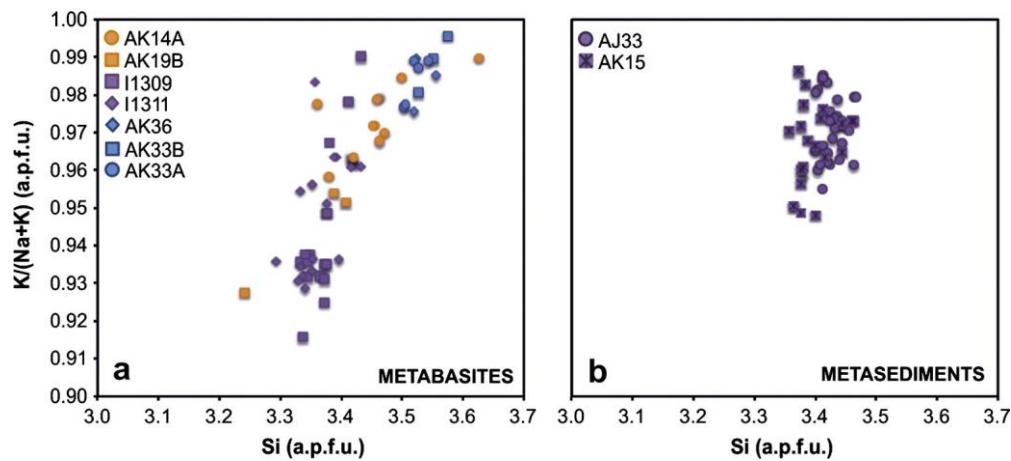

Fig. 20. Compositions of phengitc micas of metabasites (a) and metasediments (b) from Morghab Complex, Chah Gorbeh Complex and meta-pillow in the K/(Na + K) versus Si diagram.

traced in the MC to the South of the Mileh mine, where it forms a synformal setting due to an E–W trending D$_3$ fold system. Mapping of this area gave some important information on the tectonic setting of the AMC, because serpentinite slivers and thrust sheets occur in the core of a main antiformal structure across the watershed between the Mileh and Chah Gorbeh basins (Fig. 7). Serpentinites here outcrop in a sort of faulted tectonic window, indicating that large thrust tectonic slices of ultramafic rocks may floor the CGC. This also confirms that the D$_3$ folding event affected the entire accretionary wedge.

A similar setting is given by D$_3$ vertical folds, which deform thick isoclinally folded carbonate layers from the Lakh Marble and Morghab Complex. They also occur in the southern part of the Anarak massif, WNW of Anarak, in the high carbonate peaks of Kuh-e Darreh Anjir (Lakh Marble). Here the D$_3$ folds show a marked S-shape asymmetry to the west.

4.2. HP metamorphism of the Anarak accretionary wedge

The mineral assemblages and microstructural relationships described in the previous sections, indicate that all the metamorphic units of the Anarak accretionary wedge experienced relatively HP metamorphism. However, the peak blueschist facies conditions recorded by the MC, CGC and metapillows occurred in different moments of the metamorphic evolution of these rocks. Glaucophane relics are preserved only as tiny inclusions in epidote porphyroblasts in metabasites from the MC (Fig. 12), while the main foliation developed under greenschist facies conditions. A different metamorphic evolution is recorded by the metabasites from the CGC,

which show a syn-D_2 to post-D_2 growth of the peak HP paragenesis (chlorite + Fe-rich epidote + albite + magnetite + white mica + glaucophane/riebeckite). Mg-riebeckite instead grows completely static on the greenschist facies paragenesis in meta-pillows.
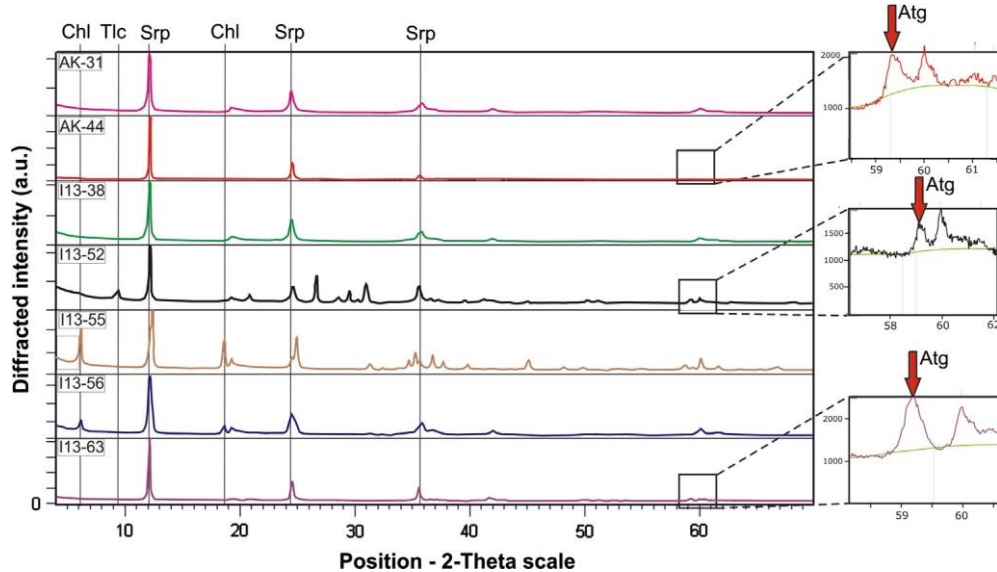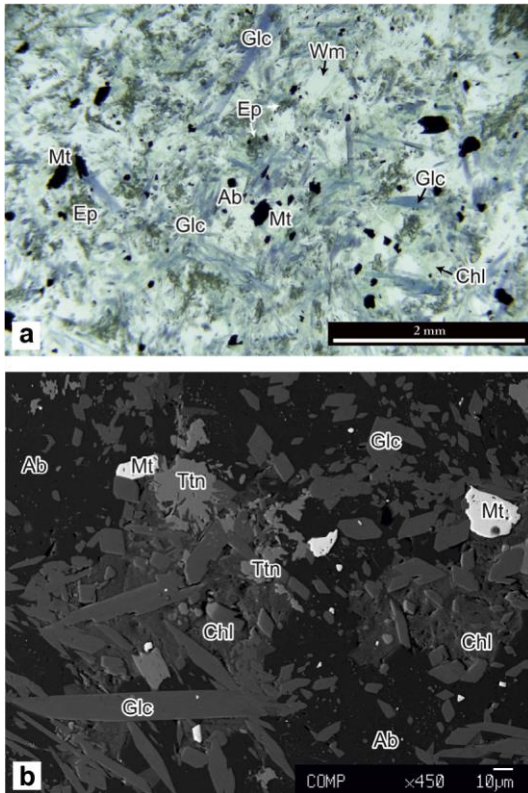

Fig. 21. XRD patterns of serpentinites. The mineralogy (Table 5) is dominated by serpentine and magnetite, with minor chlorite, clinopyroxene, olivine and carbonates.

Fig. 22. Photomicrographs of meta-pillows blueschists (transmitted light (a), and BSE image (b)) with magnetite (Mt), titanite (Ttn) and Na amphibole crystals, which statically overgrow the main foliation defined by albite and chlorite, sample AJ33.

As they form a tectonic slice interleaved within serpentinites, greenschists and later trondhjemite stocks, no direct correlation was possible with the growth of the HP paragenesis and the regional S_2 foliation of the MC and CGH.

In order to constrain the peak metamorphic conditions of the CGC metabasites and the metapillows, two isochemical P–T sections (pseudosections) have been calculated with Perple_X computer package (Connolly, 1990), using the thermodynamic database and equation of state for H_2O of Holland and Powell (1998). We used bulk compositions analyzed by XRF with FeO as total iron. The occurrence of magnetite in equilibrium with glaucophane/riebeckite-bearing mineral assemblages indicates relatively high oxygen fugacity (fO_2), in a range between the fayalite-magnetite-quartz (FMQ) and hematite-magnetite (HM) buffers. Calculation at fixed fO_2 enables to consider also the Fe^{3+}-bearing phases and the stability of equilibrium mineral assemblages and metamorphic reactions that strongly depend on this intensive variable. A forward modelling by Gibbs free energy minimization is much more correct with the use of solid solutions. However, given the uncertainties of some solid

solution models (e.g. amphibole, Tumiati et al., 2013) and the aim of this modelling, we calculated simplified pseudosections only to constrain the P–T peak conditions reached by the analyzed rocks, independently from the compositional variation of the various solid solutions.

The P–T metamorphic conditions for the CGC and pillow metabasalts (Figs. 24 and 25) have been modelled by a pseudosection calculated in the P–T range of 1–15 Kbar and 200–700 C, respectively. Both pseudosections are characterized by the occurrence of lawsonite at low temperatures (T < 300–400 C) and destabilisation of epidote at T > 400 C for sample AK33A. Note that in pseudosection of sample I1309 we also considered the stability of carbonates, given the occurrence of calcite inclusions in glaucophane (Fig. 17c). The assemblage epidote + albite + titanite + chlorite + white mica + glaucophane ± calcite, typical of CGC metabasites, is modelled by gray fields at T 350–400 C and P 7.5–8.5 Kbar (Fig. 24). The transition from actinolitic amphibole to Na-rich amphibole and the appearance of epidote in the mineral assemblage occurred at T 350 C and P 6–7 Kbar. Similar peak pressure conditions were reached by metapillow basalts, where the static growth of riebeckite on chlorite + albite + white mica + titanite ± epidote likely occurred at 8–8.5 Kbar in a temperature range slightly higher than that of the metabasites from CGC (up to 450 C; Fig. 25). Moreover, if we consider also the coexistence of static magnetite crystals along with riebeckite and the lower abundance of epidote with respect to metabasites from CGC, temperatures could reach 500 C for a peak pressure of 8 Kbar.

The metamorphic evolution of the Anarak accretionary wedge therefore records a multistage evolutionary history. Samples from MC only preserve a relatively HP relict mineral assemblage which predates the main metamorphic foliation (S2). This metamorphic
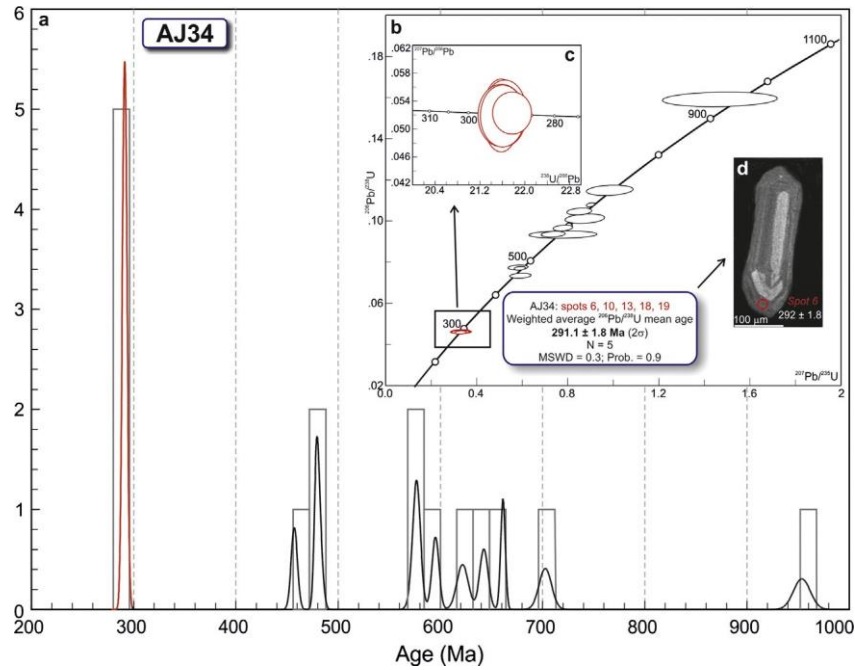
Fig. 23. (a) Relative probability diagram showing the distribution of concordant U–Pb zircon ages. (b) Conventional Concordia diagram (Wetheril, 1956) of all SHRIMP U–Pb analyses. Individual error ellipses are given at 2ř level. MSWD: Mean Square of Weighted Deviates; Prob.: Probability of fit; N = number of analyses. (c) Tera-Wasserburg Concordia diagrams (Tera and Wasserburg, 1972) displaying the youngest (Lower Permian) SHRIMP U–Pb analyses (spots 6, 10, 13, 18 and 19). Individual error ellipses are given at 2ř level. (d) CL image of a representative young (Early Permian) zircon grain. Circle represents the spot analysis; normal and italic numbers denote [206]Pb/[238]U ages
   with 1ř error and spot label, respectively.

Fig. 24. Simplified isochemical P–T section for blueschist calculated at H$_2$O and CO$_2$ saturated conditions in the system NKCFMASH(+Ti). Gray areas are the hypothetical stability fields of the main foliation in equilibrium with glaucophane for sample I1309 from the Chah Gorbeh Complex. Abbreviations: law = lawsonite, ttn = titanite, jd = jadeite, gl = glaucophane, phen = phengite, chl = chlorite, arag = aragonite, stlp = stilpnomelano, wm = white mica, FeNamp = Fe–Na-amphibole (glaucophane + riebeckite), mu = muscovite, ab = albite, kf = K-feldspar, anl = analcite, cc = calcite, lmt = laumontite, acti = actinolite, q = quartz, ep = epidote, bt = biotite, FeCaNamp = Fe–Ca–Na-amphibole, Nawm = Na-rich white mica (paragonite + muscovite), ilm = ilmenite, FeCapx = Fe–Ca-clinopyroxene, ky = kyanite, carb = calcite + dolomite, dol = dolomite, plag = plagioclase, mt = magnetite, Camp = pargasitic amphibole, rieb = riebeckite.

stage could be older than the low blueschist conditions recorded by the syn- to post-D$_2$ growth of sodic amphibole in both CGC and pillow metabasalts. This is in agreement with the structural

Fig. 25. Simplified isochemical P–T section for blueschist calculated at H$_2$O saturated conditions in the system NKCFMASH(+Ti). Gray areas are the hypothetical stability fields of the main foliation and of statical overgrown by alkali-amphibole for sample Ak33a from the blueschist meta-pillows. Abbreviations are the same as those in Fig. 24. Other abbreviations: ru = rutile, andr = andradite, vsv = vesuvianite, pump = pumepellyite.

analyses showing that the regional foliation S$_2$ is the same in both units. As portrayed by the pseudosection modelling, these two units likely recorded almost a similar P–T prograde evolution. This is confirmed by the static glaucophane crystallization in pillow metabasalts and by the Na-increase towards syn-S$_2$ amphibole rims of the MC metabasites.

The occurrence of lizardite + antigorite (see Section 3.3) in the serpentinites unit and the phengitic composition of white micas from the metasediments of the CGC and MC (Figs. 15 and 20) indicate that also these rocks experienced the same HP/LT metamorphism recorded in the metabasites. This in turn point out that tectonic units of the AMC were underplated and later exhumed as coherent terrains.

4.3. Mesozoic evolution

The Triassic evolution of the Anarak area is mainly recorded in its northern and southern parts. The Olenekian to Ladinian succession of Nakhlak, exposed to the north of Anarak (Fig. 2), records the evolution of a volcanic arc developed on continental crust in relation with the Cimmerian orogeny (Alavi et al., 1997; Balini et al., 2009; Zanchi et al., 2009b). The intermediate unit, the Baqoroq Fm. contains 1000 m of coarse continental conglomerates, eroded by an exhumed metamorphic basement (the Anarak Metamorphic Complex). Heavily altered large clasts of pinkish granitoids occur at the base.

Along the Palaeotethys suture zone south of Anarak (Figs. 1 and 2), Bagheri and Stampfli (2008) identified two low-grade units (the Doshak accretionary wedge and the Bayazeh Flysch), Permian to Triassic in age, which record the progressive closure of the Palaeotethys during the Cimmerian collision of the Yazd terrane.

Additional stratigraphic constraints on the age of deformation of the AMC come from the Khur area. Here the Shemshak Group overlies the AMC and related units, with a sharp non-conformity, suggesting an important Eo-Cimmerian tectono-metamorphic event (Sharkovski et al., 1984). In the Chah Palang region, 50 kms south of Chupanan, a thick succession of fine-grained sandstones and slates attributed to the Late Triassic–Lower Jurassic Shemshak Formation by Aistov et al. (1984) non-conformably rests with a basal conglomerate on the Permian–Triassic Doshak metamorphics (Bagheri and Stampfli, 2008). It shows an intensive contractional deformation given by NE–SW SE-verging folds and thrusts, developed under very low-grade metamorphic conditions with a striking slaty cleavage (Fig. 26). The folded Shemshak beds are in turn unconformably covered by a thick conglomerate at the base of the Chah Palang Formation, Late Jurassic (?) to Early Cretaceous in age (Aistov et al., 1984; Wilmsen et al., this vol.).

Stratigraphic relationships among these units indicate that the Palaeotethys suture closed before the deposition of the Shemshak Group, which seals the suture zone, and that a strong compression, affecting the Shemshak, occurred before the end of the Jurassic. A similar scenario is also indicated north of Torud, by the polyphase metamorphism of the Shotur Kuh Complex related to two main deformational events involving also the Shemshak Group (Rahmati-Ilkhchi et al., 2011). Stratigraphic constraints are also available in the Anarak area as Lower Cretaceous beds, that non-conformably cover some portions of the complex, give a local minimum age for the deformation. Upper Cretaceous units are more common and rest with a marked angular unconformity on the Triassic succession of Nakhlak (Balini et al., 2009; Zanchi et al., 2009b).

Sedimentological evidence (petrographic compositions, facies, and evolutionary trends) indicates that the Late Cretaceous marine transgression occurred on an extremely low relief. This observation is supported, at a local scale, by (i) the geometry of the basal unconformity surface, which is generally planar, as can be

observed in Nakhlak and in the Anarak Massif and (ii) by the high textural and mineralogical maturity of the quartzarenitic sandstone at the base of the succession. As sedimentological data indicate that the Cretaceous marine transgression occurred on a low relief area, it follows that the present-day relief developed later. The Upper Cretaceous beds consist of few decimeters to few meters of fine-grained conglomerates and sandstones, which rapidly evolve to shallow-water marine shelf carbonates. The composition of the basal sandstone is generally dominated by well-rounded quartz grains (i.e. derived from the underlying basement), whereas local grains (mostly consisting of serpentinites, marbles, metasediments) are generally rare and preserved as irregular pockets at the base of the succession. The textural and petrographic composition, very different from that expected from the metamorphic rocks presently outcropping close to the Cretaceous units, is explained by a significant distance of the source area at the time of deposition, further supported by the flat morphology of the unconformity surface.

4.4. Late Cenozoic thrusting

The Cenozoic succession also provides further constraints on the age of the reactivations of the Anarak tectonic structures. The occurrence of proximal conglomerates in the lower part of the Eocene succession confirms the presence of highs. The fine-grained facies of the Oligocene to Miocene units of shallow marine environment, covering the basal, proximal deposits of the Eocene succession (thus recording a transgressive trend) and the lateral continuity of their facies, support a low relief scenario at the time of deposition. A last tectonic stage (Late Neogene?), responsible for the present-day setting of the Anarak Massif is documented by the activation of E–W trending reverse faults displacing both the AMC and the Oligocene–Miocene succession, which is generally folded.

One of the main thrust systems related to the Tertiary deformation outcrops along the southern slope of Kuh-e Chah Gorbeh (Fig. 3). The sole thrust of this duplex overrides an Oligocene fossiliferous marine succession testifying to a late Tertiary reactivation of the shear zones of the Upper Palaeozoic accretionary wedge. A strong tectonic reworking of the whole nappe pile thus occurred
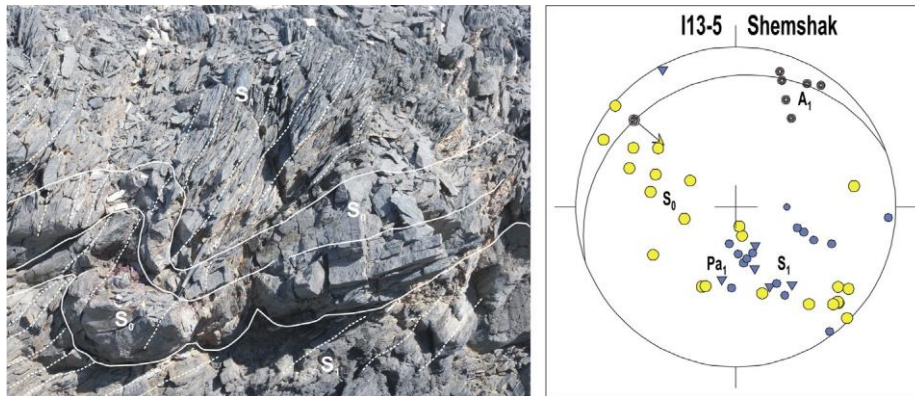
Fig. 26. Folded layers of the Shemshak Group and structural data measured in the upper part of the unit in the Chah Palang area. Note that the S_1 axial plane cleavage formed in the slates of the Shemshak is gently folded by a second deformational event.
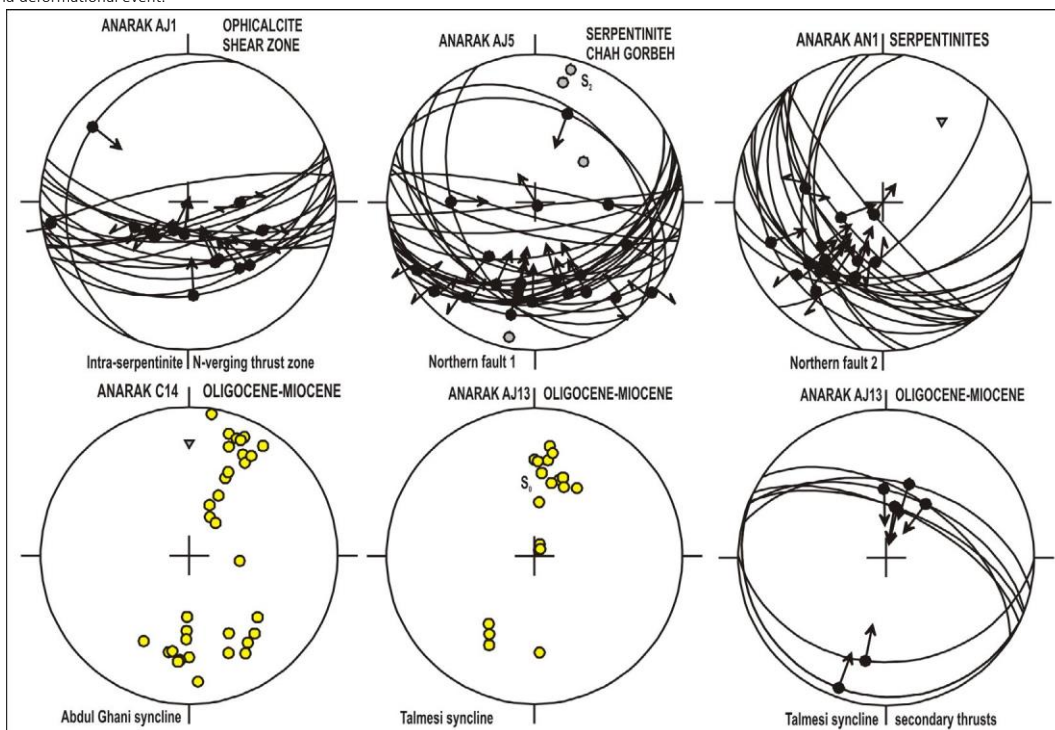
Fig. 27. Mesoscopic structural measurements of reverse fault systems thrusting the serpentinitic bodies exposed north of Anarak on the Oligocene–Miocene successions, with data on folds formed in these units. Location of sites in Fig. 2.

during Tertiary, due to E–W trending thrusts crosscutting the Palaeozoic accretionary wedge. North of Anarak, serpentinites are strongly deformed, generally showing brittle to semi-brittle fault zones superposed on their metamorphic foliations (Fig. 27). Mesoscopic fault populations measured along the ''North Anarak fault system'' consist of S-dipping N-verging reverse faults stacking the ultramafic rocks on the CGC and on the Tertiary successions. Most of the fault planes present a reverse dip-slip kinematics, but oblique and subsequent strike-slip motions also occur (Zanchi et al., 2009b).

The Eocene to the Miocene successions show open to close folds with an ESE–WSW trend, which are geometrically consistent with the shortening direction activating the reverse fault system. A regional system of folds forming the ''Abdul Ghani syncline'' (Figs. 2 and 27) is interposed between two major lenses of serpentinites, North of Anarak, and also deform the Oligocene to Miocene succession west of Anarak (AJ13, Fig. 2).

Regional thrusts and folds suggest that a significant N–S shortening occurred in Central Iran at the end of Neogene and that the present-day tectonic setting is deeply conditioned by the late Tertiary tectonics which was likely responsible for the topographic uplift of the Anarak mountain belt.

5. Discussion

5.1. Geometrical relationships between the main tectonometamorphicunits of Anarak

Based on our observations, the primary tectonic setting of the Anarak region results from the occurrence of several distinct tectono-metamorphic units, which have been coupled in an accretionary wedge during different stages of its development. This wedge mainly consists of the Morghab, Chah Gorbeh and ophiolitic complexes. Tectonic contacts preserving primary relationships among the units were subsequently refolded and crosscut by several systems of thrust faults active up to the Neogene. The MC and CGC are characterized by at least three superposed fold systems, the latter affecting the two units. Antigorite-bearing serpentinites occur in close association with the present-day lower part of the CGC. The contacts between the serpentinites and the CGC consist of thick cataclastic shear zones with ophicalcites often superimposed on ductile shear zones. A strong tectonic fragmentation is evident between the CGC and the ophiolites, and produces several tectonic slices,often reworkedbysubsequentbrittletectonics.In theinternal part of the wedge exhumed by the D_3 folds, serpentinites are clearly affected by the D_2 folds, indicating that coupling with the CGC occurred before or during this stage. The emplacement of the Lakh Marble thrust sheet occurred later, as its floor thrust cuts across the fold systems of the underlying units. Nevertheless, isoclinal folding within the LM and complex geometrical features of some portions of the thrust surface exposed south of the Kuh-e Chah Gorbeh, can suggest that this unit was also partially deformed during the D_2 folding event.

According to our reconstruction and to Sharkovski et al. (1984), the Lakh Marble forms a large thrust sheet occupying an upper structural position, because it overthrusts the Patyar, Chah Gorbeh and Morghab units, as well as the ophiolites. This interpretation differs from the hypothesis of Bagheri and Stampfli (2008), who interpreted the Lakh Marble as the autochthonous sedimentary cover of the so-called Anarak volcanic seamount. This different view on the structural position of the Lakh Marble is critical for the reconstruction of the evolution of the Anarak Massif and surrounding area. Our observations indicate that no stratigraphic relationships can be established between the Lakh Marble and the underlying units. This point suggests that carbonates of the LM are unlikely the autochthonous cover of the partially subducted Anarak seamount as suggested by Bagheri and Stampfli (2008).

5.2. Timing of metamorphism and deformation

Bagheri and Stampfli (2008) have recently defined the age of metamorphism of the Jandaq and Anarak complexes exposed between the Great Kavir Fault and the Palaeotehys suture. They suggest the occurrence of a Carboniferous ''Variscan'' event based on five ^{40}Ar–^{39}Ar radiometric ages obtained from white micas sampled from these units, clustering between 320 and 335 Ma. Two of the dated samples come from the Morghab Complex, north of Anarak, which was interpreted as a Variscan unit. The same authors obtained a poorly constrained ^{40}Ar–^{39}Ar age of 285.42 ± 1.65 Ma on crossite from the CGC, dating a second metamorphic event in HP conditions. Such event is postdated by the growth of stilpnomelane, giving an ^{40}Ar–^{39}Ar age of 232.8 ± 2.35 Ma in the Chah Gorbeh schists. In addition, they report a 262 ± 1 Ma U–Pb zircon age based on a ID/TIMS single grain analysis for an undeformed trondhjemite intruded in the CGC which should predate the subduction episode.

Our new observation, based on structural analyses, study of crosscutting relationships between intrusive and metamorphic rocks and detailed petrology, help to better define the reconstruction achieved by Bagheri and Stampfli (2008). The first point concerns the time of deformation of the MC and CGC and of the ophiolites within the Anarak accretionary wedge. We suggest that the evolution of both the MC and CGC is similar, occurring in the same HP/LT subduction-dominated geodynamic setting. A similar scenario also occurs in the Ophiolite unit, including both serpentinized ultramafic rocks and the meta-pillow basalts, which, according to our analyses, belong to an independent unit with respect to the CGC. A prograde PT path is also recorded by the meta-pillow blueschists and the occurrence of antigorite as well as structural evidence testify that the serpentinites were incorporated and subducted in the accretionary wedge before or at least during the D_2–M_2 event.

Undeformed and non-metamorphic trondhjemite stocks and dikes that intruded the AMC provide an indirect constraint for the age of metamorphism in the AMC. Bagheri and Stampfli (2008) obtained an age of 262.3 ± 1.0 Ma (U–Pb zircon) for a plagiogranite dike intruded SE of Chah Derakhtak.

Even if they considered the trondhjemites as part of the ophiolites, intrusive relationships with the country rocks unequivocally testify that trondhjemite dikes and stocks intruded after the major D_1–D_2 tectono-metamorphic stages, postdating metamorphism and deformation of the AMC accretionary wedge. Our new data suggest that these trondhjemites possibly began to intrude earlier, tracing back to Sakmarian (291.1 ± 1.8 Ma). These new geochronological results suggest that the main metamorphic and deformation stages of the CGC are likely of Carboniferous age, as proposed for the MC (Bagheri and Stampfli, 2008).

5.3. General consequences for the geodynamic evolution of Central Iran

The results of our work yield important consequences for the evolution of Central Iran. Although our reconstruction partly differs in some details from the one proposed by Bagheri and Stampfli (2008) and by Buchs et al. (2013), we agree that the whole region between Jandaq and Anarak may be part of a large allochthonous block, which was probably located in a very different tectonic position. In fact, fusulinids and brachiopods faunas of the Siah-e Godar Complex of Jandaq also indicate

a marked European affinity, as well as the Devonian age of reworked granodiorite blocks contained in the Carboniferous conglomerates of the succession (Berra et al., 2014). These units, probably deposited in a volcanic arc setting developed during the deformation of the Anarak accretionary wedge, suggest an active margin setting which is typical of the Late Palaeozoic evolution of the southern portion of Eurasia (Boulin, 1991; Schwab et al., 2004; Natal'in and Sengör, 2005; Zanchetta et al., 2013). We ascribe differences in age and composition of the AMC with respect to the Upper Palaeozoic units of NE Iran to their different geodynamic position within the collision zone. In fact, the AMC better records the evolution of the accretionary wedge, whereas the Fariman Complex and partially also the Binalood units are more closely related to the upper plate margin. On the contrary, the Upper Palaeozoic succession of both Central and North Iran records a completely different evolution, related to the extensional phenomena taking to the opening of the Neotethys ocean and to the northward drift of Iran (Angiolini et al., 2007; Gaetani et al., 2009).

Although the Nakhlak region experienced limited rotations along vertical axes since the Triassic (Muttoni et al., 2009), a major (70) counter-clockwise rotation confined to the Yazd, Tabas and Lut blocks has been recently documented during the Early Cretaceous (Mattei et al., this vol.). These paleomagnetic data strongly suggest that the westward motion of the Variscan–Cimmerian complex of Central Iran from NE Iran was probably favoured by the rotation of the Cimmerian blocks and by the concomitant opening of the Sistan and Sabzevar oceans. This induced strong right-lateral motions along a ''Mesozoic precursor'' of the Great Kavir Fault, which favoured the displacement of large crustal blocks (Barrier and Vryelinck, 2008). A pre-Pliocene dextral displacement of at least 200 km along the Great Kavir Fault System, preceding the present-day left-lateral motion of the fault (Javadi et al., 2013; Nozaem et al., 2013), is also consistent with the westward motion of the AMC and related units.

6. Conclusions

The results of our structural, petrological, geochronological and sedimentological analyses performed on the Anarak Metamorphic Complex drive to a comprehensive reconstruction of the evolution of this complex unit, allowing for a better understanding of the relationships between the ''Variscan'' and ''Cimmerian'' events in Central Iran.

Three main significant conclusions emerge from our study:

(1) The Anarak Metamorphic Complex consists of a Variscan accretionary wedge including at least three main tectonometamorphic units: the Morghab, Chah Gorbeh and ''ophiolite'' complexes, which all record a polyphase deformation developed in a subduction setting characterized by HP/LT conditions. The Lakh Marble thrust sheet, representing a widespread allochthonous nappe, is also part of the accretionary wedge and was probably coupled with the other units during the final steps of its evolution. Although the single units of the wedge show slightly different P–T-paths, the MC, CGC and meta-pillows all record a prograde blueschist equilibration, pointing to a rapid exhumation after subduction. Peak conditions obtained with pseudosections suggest T = 350–400 C and P = 9 Kbar, corresponding to an apparent temperature-depth trajectory comprised of 15 C/km.

(2) Lower Permian trondhjemite intrusive bodies, post-dating the blueschist facies metamorphism crosscut the Anarak accretionary wedge. This demonstrates that the main deformation and metamorphism occurred during the Carboniferous, as testified by previously published radiometric ages. The entire metamorphic complex may therefore represent an exhumed fragment of the Variscan wedge, which was active along the southern Eurasian margin between Turkey and Pamir at least since Devonian due to the subduction of the Palaeotethys. On the other hand, the Cimmerian units related to the closure of the suture zone occur north and south of the Carboniferous wedge of Anarak and show different characters. An intensive post-Cimmerian contractional deformation affected the whole region at several steps during Mesozoic and Cenozoic, up to recent times, dismembering the accretionary wedge of Anarak and related units.

(3) Our reconstruction confirms that the region of Anarak may represent an allochthonous displaced segment of the Palaeotethys suture zone, possibly located in the Mashhad region before the Jurassic and displaced during the opening of the Sistan-Sabzevar oceans along a precursor of the Great Kavir Fault fault in the Mesozoic. This hypothesis is also corroborated by our new data on the region of Jandaq which confirm a marked Eurasian affinity of the here exposed Upper Palaeozoic successions.

Appendix A

A.1. Analytical techniques

A.1.1. Electron probe microanalyses

Major element mineral compositions were acquired with the JEOL 8200 Superprobe (Dipartimento di Scienze della Terra, University of Milano) with wavelength dispersive spectrometers at 15 kV and 5 nA, using natural silicates as standards. A PhiRhoZ routine was used for matrix correction. Micas were measured with defocussed beam to prevent K devolatilization during the analyses. Mineral analyses were always assisted by detailed back scattered electron (BSE) images to control the microstructural site.

A.1.2. X-ray powder diffraction (XRPD)

Serpentinite samples were prepared with the side loading technique to minimize a priori preferred orientation of crystallites. The XRPD analyses were performed using a PANalytical X'Pert PRO PW3040/60 diffractometer (Department of Earth and Environmental Sciences, University of Milano-Bicocca, Italy) with Cu Kα radiation at 40 kV and 40 mA, 1 divergence, receiving and antiscattering slits, step scan of 0.02 2h and 20 s/step in the range 4–65 2h. The data analysis was performed using the PANalytical HighScore Plus software version 2.2c; the limit of detection for serpentine minerals is generally 1 wt.%. A semi-quantitative evaluation of the relative abundance of single minerals was obtained with the internal standard technique (by adding 10 wt.% of corundum powder) and the reference intensity ratio (RIR) method (Pawloski, 1985; Snyder and Bish, 1989; Wicks, 2000).

A.1.3. U–Pb zircon ages

U–Pb zircon ages have been obtained by means of SHRIMP II. Mineral separation was carried out at the Department of Earth and Environmental Sciences (University of Milano-Bicocca, Italy) following standard heavy-liquid and magnetic separation techniques. Cathodoluminescence (CL) imaging was carried out at the Beijing SHRIMP Center (CAGS, Beijing, China) by means of a HITACHI S3000-N scanning electron microscope equipped with a Gatan ChromaCL cathodoluminescence working at 15 kV, 60 İA, and 20 mm working distance.

SHRIMP II U–Pb isotopic analyses were performed at the Beijing SHRIMP Center, Institute of Geology (CAGS, Beijing). Instrumental conditions and data acquisition were generally as described by Compston et al. (1992) and Williams (1998 and reference therein). Temora (416.8 ± 1.1 Ma; Black et al., 2003) and M257 (561.3 ± 0.3 Ma, U 840 ppm, Th/U 0.27; Nasdala et al., 2008) reference zircons were used for inter-element fractionation and U concentration, respectively. The beam size was 20 İm. The analyses were corrected for common Pb using measured ^{204}Pb following Williams (1998). The common Pb composition was obtained according to the Stacey and Kramers (1975) model. The $_{235}$

U decay constant used for age calculation is after Schoene et al. (2006), whereas the ^{238}U one is after the IUGS Subcommission on Geochronology (Steiger and Jäger, 1977). Data evaluation and age calculation were done using Squid 1.02 (Ludwig, 2003a) and Isoplot/Ex3 (Ludwig, 2003b) add-in programs, respectively. All analytical data are presented in Table 6. Errors given for individual analyses are at 1ŕ level.

References

Aistov, L., Melnikov, B., Krivyakin, B., Morozov, L., 1984. Geology of the Khur area (Central Iran). Explanatory text of the Khur Quadrangle Map 1:250,000, 132 pp.

Alavi, M., 1991. Sedimentary and structural characteristics of the Paleo-Tethys remnants in northeaster Iran. Geol. Soc. Am. Bull. 103, 983–992.

Alavi, M., Vaziri, H., Seyed Enami, K., Lasemi, Y., 1997. The Triassic and associated rocks of the Nakhlak and Aghdarband areas in central and northeastern Iran as remnants of the southern Turanian active continental margin. Geol. Soc. Am. Bull. 109, 1563–1575.

Angiolini, L., Gaetani, M., Muttoni, G., Stephenson, M.H., Zanchi, A., 2007. Tethyan oceanic currents and climate gradients 300 my ago. Geology 35, 1071–1074.

Bagheri, S., Stampfli, G.M., 2008. The Anarak, Jandaq and Posht-e-Badam metamorphic complexes in Central Iran: new geological data, relationships and tectonic implications. Tectonophysics 451, 123–155.

Balini, M., Nicora, A., Berra, F., Garzanti, F., Levera, M., Mattei, M., Muttoni, M., Zanchi, A., Bollati, I., Larghi, C., Zanchetta, S., Salamati, R., Mossavvari, F., 2009. The Triassic stratigraphic succession of Nakhlak (Central Iran), a record from an active margin. In: Brunet, M.F., Wilmsen, M., Granath, J.W. (Eds.), South Caspian to Central Iran Basins. Geological Society of London Special Publications 312, pp. 287–321.

Barrier, E., Vryelinck, B., 2008. Palaeotectonic Maps of the Middle East, Atlas of 14 Maps. CGMW/CCGM, Paris, France.

Berberian, M., King, G., 1981. Toward a paleogeographic and tectonic evolution of Iran. Can. J. Earth Sci. 18, 210–265.

Berra, F., Zanchi, A., Nawab, A., 2007. Late Cretaceous transgression on a Cimmerian high (Neka Valley, Eastern Alborz, Iran): a geodynamic event recorded by glauconitic sands. Sed. Geol. 199, 189–204.

Berra, F., Zanchi, A., Malaspina, N., Javadi, H.R., Kouhpeyma, M., Angiolini, L., Vachard, D., Zanchetta, S., 2014. Evidence for an Upper Palaeozoic NorthPalaeotethyan succession in Central Iran: the Siah Godar Complex of Jandaq. Geophys. Res. Abstracts 16, EGU2014-9929-1.

Black, L.P., Kamo, S.L., Allen, C.M., Aleinikoff, J.N., Davis, D.W., Korsch, R.J., Foudoulis, C., 2003. Temora 1: a new zircon standard for Phanerozoic U–Pb geochronology. Chem. Geol. 200, 155–170.

Boulin, J., 1991. Structures in Southwest Asia and evolution of the eastern Tethys. Tectonophysics 196, 211–268.

Buchs, D.M., Bagheri, S., Martin, K., Hermann, J., Arculus, R., 2013. Paleozoic to Triassic ocean opening and closure preserved in Central Iran: constraints from the geochemistry of meta-igneous rocks of the Anarak area. Lithos 172–173, 267–287.

Compston, W., Williams, I.S., Kirschvink, J.L., Zhang, Z., Ma, G., 1992. Zircon U–Pb ages for the Early Cambrian time-scale. J. Geol. Soc. London 149, 171–184.

Connolly, J.A.D., 1990. Multivariable phase diagrams: an algorithm based on generalized thermodynamics. Am. J. Sci. 290, 666–718.

Davouzadeh, M., Weber-Diefenbach, K., 1987. Contribution to paleogeography, stratigraphy and tectonics of the Upper Paleozoic in Iran. Neues Jahrb. Geol. Palaeontol. 175, 121–146.

Evans, B.W., 2004. The serpentinite multisystem revisited: chrysotile is metastable. Int. Geol. Rev. 46, 479–506.

Fürsich, F.T., Wilmsen, M., Seyed-Emami, K., Majidifard, M.R., 2009. Lithostratigraphy of the Upper Triassic–Middle Jurassic Shemshak Group of northern Iran. In: Brunet, M.F., Wilmsen, M., Granath, J.W. (Eds.), South Caspian to Central Iran Basins. Geological Society of London Special Publications 312, pp. 129–160.

Gaetani, M., Angiolini, L., Ueno, K., Nicora, A., Stephenson, M.H., Sciunnach, D., Rettori, R., Price, G.D., Sabouri, J., 2009. Pennsylvanian_Early Triassic stratigraphy in the Alborz Mountains (Iran). In: Brunet, M.F., Wilmsen, M., Granath, J.W. (Eds.), South Caspian to Central Iran Basins. Geological Society of London Special Publications 312, pp. 79–128.

Ghasemi, A.M., Talbot, C.J., 2006. A new tectonic scenario for the Sanandaj-Sirjan Zone (Iran). J. Asian Earth Sci. 26, 683–693.

Holland, T.J.B., Powell, R., 1998. An internally consistent thermodynamic data set for phases of petrologic interest. J. Metamorph. Geol. 16, 309–343.

Horton, B.K., Hassanzadeh, J., Stockli, D.F., Axen, G.J., Gillis, R.J., Guest, B., Amini, A., Fakhari, M.D., Zamanzadeh, S.M., Grove, M., 2008. Detrital zircon provenance of Neoproterozoic to Cenozoic deposits in Iran: implications for chronostratigraphy and collisional tectonics. Tectonophysics 451, 97–122.

Javadi, H.R., Ghassemi, M.R., Shahpasandzadeh, M., Guest, B., Ashtiani, M.E., Yassaghi, A., Kouhpeyma, M., 2013. History of faulting on the Doruneh Fault System: implications for the kinematic changes of the Central Iranian Microplate. Geol. Mag., 22. http://dx.doi.org/10.1017/S0016756812000751.

Kargaranbafghi, F., Neubauer, F., Genser, J., Faghih, A., Kusky, T., 2012. Mesozoic to Eocene ductile deformation of western Central Iran: from Cimmerian collisional orogeny to Eocene exhumation. Tectonophysics 564–565, 83–100.

Kydonakis, K., Kostopoulos, D., Poujol, M., Brun, J.-P., Papanikolaou, D., Paquette, J.L., 2014. The dispersal of the Gondwana Super-fan System in the eastern Mediterranean: new insights from detrital zircon geochronology. Gondwana Res. 25, 1230–1241.

Leake, B.E., Woolley, A.R., Arps, C.E.S., Birch, W.D., Gilbert, M.C., Grice, J.D., Hawthorne, F.C., Kato, A., Mandarino, J.A., Maresch, W.V., Nikel, E.H., Rock, N.M.S., Schumacher, J.C., Smith, D.C., Stephenson, N.C.N., Ungaretti, L., Whittaker, E.J.W., Youzhi, G., 1997. Nomenclature of amphiboles: report of the subcommittee on Amphiboles of the International Mineralogical Association, Commission on New Minerals and Mineral Names. Am. Mineral. 82, 1019–1037.

Leven, E.J., Gorgij, M.N., 2006. Upper Carboniferous-Permian stratigraphy and fusulinids from the Anarak region, Central Iran. Russ. J. Earth Sci. 8, ES2002. http://dx.doi.org/10.2205/2006ES000200.

Ludwig, K.R., 2003a. A User's Manual for Isoplot/Ex 3. A Geochronological Toolkit for Microsoft Excel. Berkeley Geochronological Center Special Publication 4.

Ludwig, K.R., 2003b. SQUID 1.02. A User's Manual. Berkeley Geochronological Center Special Publication 2.

Masoodi, M., Yassaghi, A., Sadat, M.A.A.N., Neubauer, F., Bernroider, M., Friedl, G., Genser, J., Houshmandzadeh, A., 2013. Cimmerian evolution of the Central Iranian basement: evidence from metamorphic units of the Kashmar-Kerman Tectonic Zone. Tectonophysics 588, 189–208.

Mattei, M., Cifelli, F., Muttoni, G., Zanchi, A., Berra, F., Mossavvari, F., Eshraghi, S.A., 2012. Neogene block-rotation in Central Iran: evidence from paleomagnetic data. Geol. Soc. Am. Bull.. http://dx.doi.org/10.1130/B30479.1.

Moghadam, H.S., Khademi, M., Hu, Z., Stern, R.J., Santos, J.F., Wu, Y., 2013. Cadomian (Ediacaran–Cambrian) arc magmatism in the ChahJam–Biarjmand metamorphic complex (Iran): magmatism along the northern active margin of Gondwana. Gondwana Res.. http://dx.doi.org/10.1016/j.gr.2013.10.014.

Moghadam, H.S., Xian-Hua Li, X.-H., Xiao-Xiao Ling, X.-X., Stern, R.J., Zaki Khedr, M.Z., Chiaradia, M., Ghorbani, G., Arai, S., Tamura, A., 2014. Devonian to Permian evolution of the Paleo-Tethys Ocean: new evidence from U–Pb zircon dating and Sr–Nd–Pb isotopes of the Darrehanjir–Mashhad ''ophiolites'', NE Iran. Gondwana Res.. http://dx.doi.org/10.1016/j.gr.2014.06.009.

Muttoni, M., Mattei, M., Balini, M., Zanchi, A., Gaetani, M., Berra, F., 2009. The drift history of Iran from the Ordovician to the Triassic. In: Brunet, M.F., Wilmsen, M., Granath, J.W. (Eds.), South Caspian to Central Iran Basins. Geological Society of London Special Publications 312, pp. 7–29.

Nasdala, L., Hofmeister, W., Norberg, N., Mattinson, J.M., Corfu, F., Dörr, W., Kamo, S.L., Kennedy, A.K., Kronz, A., Reiners, P.W., Frei, D., Kosler, J., Wan, Y., Götze, J., Häger, T., Kröner, A., Valley, J.W., 2008. Zircon M257—a homogeneous natural reference material for the ion microprobe U–Pb analysis of zircon. Geostand. Geoanal. Res. 32, 247–265.

Natal'in, B.A., Sengör, A.M.C., 2005. Late Palaeozoic to Triassic evolution of the Turan and Scythian platforms: the pre-history of the Palaeo-Tethyan closure. Tectonophysics 404, 175–202.

Nozaem, R., Mohajjel, M., Rossetti, F., Della Seta, M., Vignaroli, G., Yassaghi, A., Salvini, F., Eliassi, M., 2013. Post-Neogene right-lateral strike-slip tectonics at the north-western edge of the Lut Block (Kuh-e–Sarhangi Fault), Central Iran. Tectonophysics 589, 220–233.

Omrani, H., Moazzen, M., Oberheansli, R., Tsujimori, T., Bousquet, R., Moayyed, M., 2013. Metamorphic history of glaucophane–paragonite–zoisite eclogites from the Shanderman area, northern Iran. J. Metamorph. Geol. 31, 791–812.

Pawloski, G.A., 1985. Quantitative determination of mineral content of geological samples by X-ray diffraction. Am. Mineral. 70, 663–667.

Rahmati-Ilkhchi, M., Jeřábek, P., Faryad, S.W., Koyi, H.A., 2011. Mid-Cimmerian, Early Alpine and Late Cenozoic orogenic events in the Shotur Kuh metamorphic complex, Great Kavir block, NE Iran. Tectonophysics 494, 101–117.

Ruttner, A.W., 1993. Southern borderland of Triassic Laurasia in north-east Iran. Geol. Rundsch. 82, 110–120.

Schoene, B., Crowley, J.L., Condon, D.J., Schmitz, M.D., Bowring, S.A., 2006. Reassessing the uranium decay constants for geochronology using ID-TIMS U–Pb data. Geochim. Cosmochim. Acta 70 (2), 426–445.

Schwab, M., Ratschbacher, L., Siebel, W., McWilliams, M., Lutkov, V., Minaev, V., Chen, F., Stanek, K., Nelson, B., Frisch, W., Wooden, J.L., 2004. Assembly of the Pamirs: age and origin of magmatic belts from the southern Tien Shan to the southern Pamirs and their relation to Tibet. Tectonics 23, TC4002. http:// dx.doi.org/10.1029/2003TC001583.

Schwartz, S., Guillot, S., Reynard, B., Lafay, R., Debret, B., Nicollet, C., Lanari, P., Auzende, A.L., 2013. Pressure-temperature estimates of the lizardite/antigorite transition in high pressure serpentinites. Lithos 178, 197–210.

Sengör, A.M.C., 1979. Mid-Mesozoic closure of Tethys and its implications. Nature 279, 590–593.

Sharkovski, M., Susov, M., Krivyakin, B., 1984. Geology of the Anarak area (Central Iran). Explanatory Text of the Anarak Quadrangle Map 1:250000. Geological Survey of Iran, V/O ''Tecnoexport'' USSR Ministry of Geology Reports, 19.

Sheikholeslami, M.R., Kouhpeyma, M., 2012. Structural analysis and tectonic evolution of the eastern Binalud Mountains, NE Iran. J. Geodyn. 61, 23–46.

Snyder, R.L., Bish, D.L., 1989. Quantitative analysis. In: Bish, D.L., Posts, J.E. (Eds.), Modern Powder Diffraction. Mineralogical Society of America, Reviews in Mineralogy and Geochemistry 201, pp. 101–144.

Soffel, H.C., Eftekhar-Nezhad, J., Hushmandzadeh, A., 1996. New palaeomagnetic data from Central Iran and a Triassic palaeoreconstruction. Geol. Rundschau 85, 293–302.

Stacey, J.S., Kramers, J.D., 1975. Approximation of terrestrial lead isotope evolution by a 2-stage model. Earth Planet. Sci. Lett. 26, 207–221.

Stampfli, G.M., Borel, G.D., 2002. A plate tectonic model for the Paleozoic and Mesozoic constrained by dynamic plate boundaries and restored synthetic oceanic isochrones. Earth Planet. Sci. Lett. 196, 17–33.

Stampfli, G.M., Marcoux, J., Baud, A., 1991. Tethyan margins in space and time. Palaeogeogr., Palaeoclimatol., Palaeoecol. 87, 373–409.

Steiger, R.H., Jäger, E., 1977. Subcommission on geochronology: convention on the use of decay constants in geo- and cosmochronology. Earth Planet. Sci. Lett. 36, 359–362.

Stöcklin, J., 1974. Possible ancient continental margins in Iran. In: Burk, C.A., Drake, C.L. (Eds.), The Geology of Continental Margins. Springer-Verlag, Berlin, pp. 873–887.

Tera, F., Wasserburg, G., 1972. U–Th–Pb systematics in three Apollo 14 basalts and the problem of initial Pb in lunar rocks. Earth Planet. Sci. Lett. 14, 281–304.

Torabi, G., 2011. Late Permian blueschist from Anarak ophiolite (Central Iran, Isfahan province), a mark of multi-suture closure of the Paleo-Tethys Ocean. Rev. Mexicana Ciencias Geol. 28, 544–554.

Torabi, G., 2012. Late Permian post-ophiolitic trondhjemites from Central Iran: a mark of subduction role in growth of Paleozoic continental crust. Island Arcs 21, 215–229.

Torsvik, T.H., Cocks, R.M., 2004. Earth geography from 400 to 250 Ma: a paleaomagnetic, faunal and facies review. J. Geol. Soc. London 161, 555–572.

Tumiati, S., Fumagalli, P., Tiraboschi, C., Poli, S., 2013. An experimental study on COH-bearing peridotite up to 3.2 GPa and implications for crust-mantle recycling. J. Petrol. 54, 453–479.

Ulmer, P., Trommsdorff, V., 1995. Serpentinite stability to mantle depths and subduction related magmatism. Science 268, 858–861.

Wendt, J., Kaufmann, B., Belka, Z., Farsan, N., Bavandpur, A.K., 2005. Devonian/Lower Carbonifeous stratigraphy, facies patterns and palaeogeography of Iran Part II. Northern and Central Iran. Acta Geol. Pol. 55 (1), 31–97.

Wetheril, G.W., 1956. Discordant uranium-lead ages. Trans. Am. Geophys. Union 37, 320–326.

Wicks, F.J., 2000. Status of the reference X-ray powder-diffraction patterns for the serpentine minerals in the PDF database—1997. Powder Diffract. 15, 42–50.

Wicks, F.J., O'Hanley, D.S., 1988. Serpentine minerals: structures and petrology In Bailey, SW Hydrous phyllosilicates (exclusive of micas). Mineral. Soc. Am., Rev. Mineral. Geochem. 19, 91–167.

Williams, I.S., 1998. U–Th–Pb geochronology by ion microprobe. In: McKibben, M.A., Shanks III, W.C., Ridley, W.I. (Eds.), Applications of Microanalytical Techniques to Understanding Mineralizing Processes. Reviews of Economy Geology 7, pp. 1–35.

Wilmsen, M., Fursich, F.T., Taheri, J., 2009. The Shemshak Group (Lower–Middle Jurassic) of the Binalud Mountains, NE Iran: stratigraphy, depositional environments and geodynamic implications. In: Brunet, M.F., Wilmsen, M., Granath, J.W. (Eds.), South Caspian to Central Iran Basins. Geological Society of London Special Publications 312, pp. 175–188.

Wunder, B., Schreyer, W., 1997. Antigorite: high pressure stability in the system MgO–SiO₂–H₂O (MSH). Lithos 41, 213–227.

Zanchetta, S., Zanchi, A., Villa, I., Poli, S., Muttoni, G., 2009. The Shanderman eclogites: a Late Carboniferous high-pressure event in the NW Talesh Mountains (NW Iran). In: Brunet, M.F., Wilmsen, M., Granath, J.W. (Eds.), South Caspian to Central Iran Basins. Geological Society of London Special Publications 312, pp. 57–78.

Zanchetta, S., Berra, F., Zanchi, A., Bergomi, M., Caridroit, M., Nicora, M., Heidarzadeh, G., 2013. The record of the Late Palaeozoic active margin of the Palaeotethys in NE Iran: constraints on the Cimmerian orogeny. Gondwana Res. 24, 1237–1266.

Zanchi, A., Zanchetta, S., Berra, F., Mattei, M., Garzanti, E., Molyneux, S., Nawab, A., Sabouri, J., 2009a. The Eo-Cimmerian (Late? Triassic) orogeny in north Iran. In: Brunet, M.F., Wilmsen, M., Granath, J.W. (Eds.), South Caspian to Central Iran Basins. Geological Society of London Special Publications 312, pp. 31–55.

Zanchi, A., Zanchetta, S., Garzanti, E., Balini, M., Berra, F., Mattei, M., Muttoni, G., 2009b. The Cimmerian evolution of the Nakhlak-Anarak area, Central Iran, and its bearing for the reconstruction of the history of the Eurasian margin. In: Brunet, M.F., Wilmsen, M., Granath, J.W. (Eds.), South Caspian to Central Iran Basins. Geological Society of London Special Publications 312, pp. 261–286.